Gaseous fluidization of short fibers and SiC powders, influence of temperature and pressure

Thomas Da Calva Mouillevois, Clément Rivière, Georges Chollon, Gérard Vignoles, Nathalie Bertrand

Gaseous fluidization of short fibers and SiC powders, influence of temperature and pressure

CRediT authorship contribution statement

- 1st author: **Thomas Da Calva**[1,2] *(corresponding author)*: dacalva@lcts.u-bordeaux.fr, Conceptualization, Methodology, Software, Formal analysis, Investigation, Writing - Original Draft, Visualization
- 2nd author: **Clément Rivière**[2]: clement.riviere.1@etu.u-bordeaux.fr, Investigation, Writing - Original Draft
- 3rd author: **Georges Chollon**[1]: chollon@lcts.u-bordeaux.fr, Validation, Writing - Review & Editing
- 4th author: **Gerard Vignoles**[1,2]: vinhola@lcts.u-bordeaux.fr, Methodology, Formal analysis, Writing - Review & Editing
- 5th author: **Nathalie Bertrand**[1,2]: bertrand@lcts.u-bordeaux.fr, Validation, Writing - Review & Editing, Supervision, Project administration

[1] *ThermoStructural Composites Laboratory (LCTS), 3 Allée de la Boétie, 33600 Pessac, France*

[2] *University of Bordeaux, 351 Cour de la Libération, 33400 Talence, France*

Highlights

- Fluidization of a mixture of short fibers and SiC powder.
- Calculation of the minimum fluidization velocity (U_{mf}) for rarefied/laminar flows.
- Validation of the calculated U_{mf} values by measurements at various pressures and temperatures.
- Optimization of the fluidization conditions for a short fiber/powder mixture.
- PyC ex-ethanol CVD coating deposition on short fiber/powder mixtures.

Graphical abstract

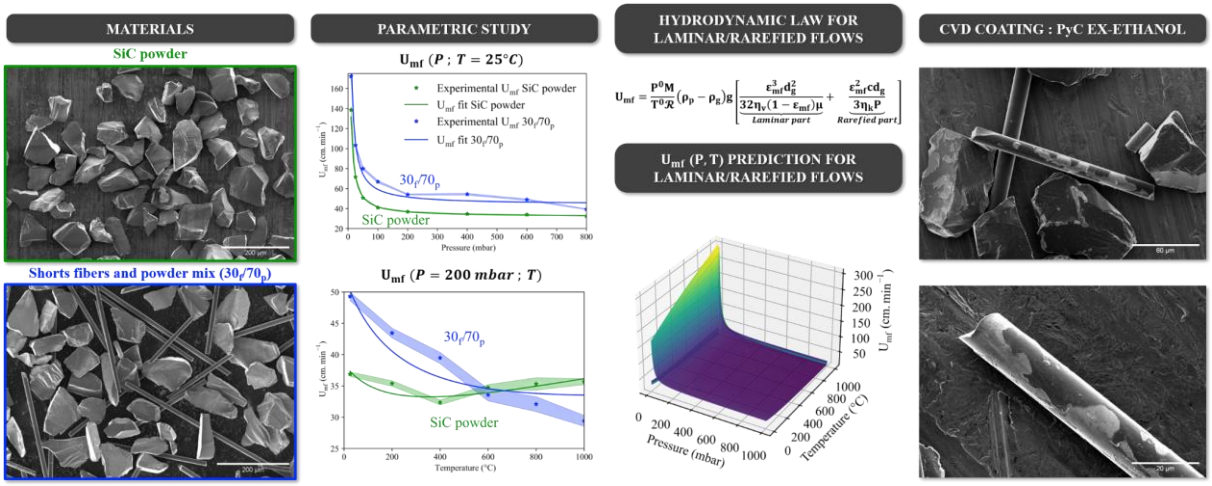

Colors for figures

For a good reading of the figures, all require color printing.

Abstract

The fluidization of short Hi Nicalon S fibers was investigated before considering CVD coatings with controlled composition and thicknesses. The fluidization of a short fiber batch alone being delicate and not reproducible, the study consisted in comparing the hydrodynamic behavior of a powder alone, to that of a short fiber/powder mixture. The fluidization behavior of the particle beds was studied by following their pressure drop as a function of pressure and temperature. The minimum fluidization velocity (U_{mf}) was evaluated at room temperature (T_{amb}) at different reduced pressures, and at 200 mbar as a function of temperature. The results are in good agreement with the theoretical equations. At low pressures and T_{amb}, U_{mf} increases rapidly. In contrast, U_{mf} varies only slightly with temperature. While the pressure does not seem to affect the fluidization behavior of the powder alone, it displays a clear optimum at 200 mbar for the short fiber/powder mixture.

Keywords

Fluidized bed, Short fibers, SiC powder, Temperature, Pressure, Hydrodynamic

Nomenclature

Archimedes number	Ar	(-)
Gas molecular velocity	c	($m.s^{-1}$)
Average particle diameter	d_g	(m)
Knudsen diffusion coefficient	D_K	($m^2.s^{-1}$)
Average equivalent hydraulic pore diameter	d_p	(m)
L^2 norm	E_{L^2}	(-)
Gravitational force constant	g	(9.81 $m.s^{-2}$)
Bed height	H	(m)
Normalized bed height	H^*	(-)
Bed height at minimum fluidization velocity	H_{mf}	(m)
Hausner ratio	HR	(-)
Mass flux	j	($kg.m^2.s^{-1}$)
Permeability	K	(m^2)
Apparent permeability	K_{app}	(m^2)
Kozeny-Carman constant	K_{KC}	(-)
Knudsen number	Kn	(-)
Mass of the bed	m	(kg)
Molar mass	M	($kg.mol^{-1}$)
Pressure	P	(Pa)
Reference pressure	P^0	(=101325 Pa)
Pressure under the bed	P^+	(Pa)
Pressure above the bed	P^-	(Pa)
Normalized bed pressure drop	ΔP^*	(-)
Fluidization quality factor (normalized bed pressure drop plateau)	ΔP^*_∞	(-)

Pressure drop generated by the particle bed (taken as positive)	$\Delta P_{bed} = P^+ - P^-$	(Pa)
Average pressure	P_{mean}	(Pa)
Theoretical pressure drop	$\Delta P_{theoretical}$	(Pa)
Flow rate	Q	($m^3.s^{-1}$)
Universal constant of perfect gases	$\mathcal{R}$	(~8.314 $J.K^{-1}.mol^{-1}$)
Particle Reynolds number at minimum fluidization velocity	Re_{mf}	(-)
Cross section of the fluidization column	S	(m^2)
Specific surface area	S_s	($m^2.kg^{-1}$)
Internal surface area	S_v	($m^2.m^{-3} = m^{-1}$)
Absolute temperature	T	(K)
Reference temperature	T^0	(= 273.15 K)
Room temperature	T_{amb}	(K)
Surface velocity of the gas	U	($m.s^{-1}$)
Minimum fluidization velocity	U_{mf}	($m.s^{-1}$)
Coefficient for bed expansion correlation	α	(-)
Coefficient for bed expansion correlation	β	(-)
Bed porosity	ε	(-)
Bed porosity at minimum fluidization velocity	ε_{mf}	(-)
Viscous tortuosity	η_v	(-)
Knudsen tortuosity	η_K	(-)
Mean free path	λ	(m)
Viscosity	μ	(Pa.s)
Mass density	ρ	($kg.m^{-3}$)
Density of the carrier gas	ρ_g	($kg.m^{-3}$)
Density of the particles	ρ_p	($kg.m^{-3}$)
Solid volume fraction	ϕ	(-)
Particle sphericity	ψ_s	(-)

1. Introduction

The improvement of the performances of aircraft engines and the reduction of their environmental impact can be achieved by both reducing material weight and enhancing the engine efficiency, i.e. by increasing operation temperature. Ceramic matrix composites (CMCs) reinforced with continuous fibers offer low density, high fracture strength, creep resistance and toughness. These properties are maintained at high temperatures in corrosive atmospheres, making CMCs suitable for use in the combustion environments of aircraft engines or gas turbines [1,2]. CMCs based on silicon carbide (SiC) fibers, a pyrolytic carbon (pyC) or boron nitride (BN) interphase, and a SiC matrix have shown promise in replacing nickel-based superalloys in these applications [3].

A new generation of discontinuous reinforcement materials is currently being under development. Short-fiber CMCs are designed for specific purposes, where the weaving of long fibers is not possible, or where more isotropic properties are required. The shaping and densification of these materials do not involve weaving or impregnation of the fabrics, but rather processes inspired by powder metallurgy. However, short-fiber CMCs must preserve their

damageable character; this can be ensured by adding an interphase between the fibers and the matrix acting as a mechanical fuse. The fluidized bed chemical vapor deposition (FB-CVD) process offers the possibility to coat particles with a uniform thickness deposit. The fluidization process, which has long been used in industry for a wide range of applications, has been rapidly combined with CVD techniques using radiative, plasma, microwave heating, etc. [4–6]. These methods offer a wide range of applications, for various types of powder substrates and a large choice of deposited materials (Ni, Fe, W, Cu, Al, Al_2O_3, Ti, Co, HfW_2... [7]). Moreover, they exhibit higher yield compared to classical CVD techniques.

The gaseous fluidization of particles with a form factor close to 1 has been extensively investigated. These particles can be of nanometric, submicronic or micrometric size [8,9], dense or porous [10,11], and of varied chemical nature (W, AlN, TiB_2, TiO_2, Al, Al_2O_3, SiC, WC, C, ... [7,9,12]). In general, very fine particles, of group C according to Geldart's classification (typically flour or cement), tend to be cohesive and are therefore difficult to fluidize. Conversely, large and dense particles, of group D (such as lead shot), tend to splash inside the fluidized bed chamber. The large majority of fluidized bed systems use group A and B powders because of their hydrodynamic behavior, which is well suited to fluidization [13]. Short fibers, cylindrical in shape and with a form factor of the order of a few tens, can't be included in the Geldart's classification. A few works mention the fluidization of short carbon fibers [5,6,14,15], but their experimental hydrodynamic fluidization behavior has not been experimentally characterized. Some authors have explored the fluidization behavior of rod-like particles or mixtures of rod-like and near-spherical particles. These studies used Computational Fluid Dynamic/Discrete Element Method (CFD-DEM) approaches [16–21] and some of them even tried to validate the models with experimental tests [16,19,20]. In the latter case, the diameters and lengths of the particles were very different from those of the fine and short fibers considered in the present study (millimetric instead of micrometric). The resulting behavior may therefore be very different from that encountered in the present study.

When a granular load is cohesive and difficult to fluidize, it is possible to improve the fluidization behavior by adding large particles of group A or B. The presence of these large particles acts as a mechanical agitator within the bed. The material constituting the coarse particles must obviously be compatible with the process [22]. According to Dutta and Dullea [23] and Alavi and Caussat [24], the addition of large particles, whose fluidization is well controlled, allows a reduction in the inter-particle forces, which leads to a change in the overall structure of the powder bed. Indeed, the fluidization of large particles creates a local agitation which leads to the destruction of agglomerates or preferential gas paths. Moreover, the efficiency of this technique largely depends on the properties of the easy-to-fluidize particles (size and density) and their proportion in the mixture [25,26]. For example, Liu *et al.* [26] studied the effect of adding two types of coarse particles to two different types of fine powders. The experimental results show that the two fine powders do not react identically to the same addition of coarse particles. Zhou and Li [25], on the other hand, showed that fluidization of a mixture of a fine powder (5 µm) with 200 µm coarse particles is achievable if the proportion of fine particles does not exceed approximately 33% by weight of the mixture. The existence of a minimum proportion of large particles is thus demonstrated.

Hydrodynamic parameters of interest include: minimum fluidization velocity (U_{mf}), bed porosity at the fluidization minimum (ε_{mf}), bed pressure drop (ΔP_{bed}) and bed expansion (H/H_{mf}) as a function of the gas velocity (U). Even though fluidized bed reactors are most often operated at gas velocities well above the minimum fluidization velocity on an industrial scale, this characteristic has a double interest. Firstly, it is a practical criterion of the

fluidization process and the dimensioning of these reactors. Secondly, it is an essential quantity for a theoretical approach of fluidization. The fluidization minimum velocity (U_{mf}) can indeed be linked via models to the characteristics of the fluid and the particle load, and the expansion of the bed can itself be correlated to theoretical or empirical models.

The temperature (T) and pressure (P) of the gas are essential parameters for the CVD process, but they are also critical for the fluidization behavior of the load. Both the temperature and pressure influence the fluidization behavior of the gas-particle system via the density and viscosity of the gas. Many studies indicate that the behavior of pressure depends on the particle size. Experimental results show a decrease of the minimum fluidization velocity with increasing pressure for particles larger than 100 µm (particles of category B and D according to Geldart). In contrast, for fine particles (Geldart category A), the minimum fluidization velocity is not affected by pressure [27]. Temperature can also have a significant effect on the inter-particle forces. The influence of temperature on U_{mf} also depends on the particle size, which itself defines the type of gas-particles interaction. In general, most predictions of the fluidization behavior at high temperature are only based on the changes in the gas properties. This approach is merely valid if only hydrodynamic forces control the fluidization behavior.

The present work aims to characterize the fluidization behavior of a bed consisting of a mixture of SiC short fibers and SiC powder, via a detailed hydrodynamic study. The SiC powder is used as a "fluidizing agent" for the short fibers. This powder is on the borderline between the A and B categories of the Geldart classification and thus meets the prerequisite of an easy fluidization. With the ultimate goal of achieving ceramic coatings on short fiber/powder mixtures in a fluidized bed CVD reactor, it is necessary to control and, if possible, to predict the fluidization behavior of such feedstock. A theoretical approach is first proposed to describe the influence of pressure, temperature and bed geometry characteristics on the gas flow and bed expansion. Then, experimental results are presented in a second part and later discussed.

2. Materials and methods

2.1. Influence of the pressure

Most of the research on the effect of pressure on gaseous fluidization phenomena has been conducted at pressures above 1 bar [27–29]. The authors report a dependence between the pressure effect and the size of the fluidized particles. Generally speaking, for particles smaller than 100 µm, the pressure has a limited impact on the minimum fluidization velocity while for particles larger than 100 µm, the authors observe a decrease of U_{mf} as the pressure increases. The experimental results are explained by Rowe *et al.* [30] who modified the Ergün equation [31] to express the minimum fluidization velocity in terms of particle size and density, as well as gas density and viscosity. Among these authors, a number have been interested in predicting the behavior of U_{mf} as a function of pressure and particle size. Most of the works (conducted above and below 1 bar) apply the Ergün equation to determine the fluidization behavior, as a function of pressure, through the density of the carrier gas. However, the Ergün equation assumes the knowledge of the bed porosity at the minimum fluidization velocity (ε_{mf}) and the sphericity of the particles (ψ_s), two characteristics that are sometimes difficult to evaluate. Many studies [32–36] propose correlation coefficients which avoid the assumptions made on ε_{mf} and ψ_s, but the multiplicity of these coefficients, specific to the nature of the fluidized bed, make the correlations poorly reliable. Moreover, it is important to note that the proposed correlations are only valid in the case of laminar and inertial flow.

Some studies focus on the influence of reduced pressures on U_{mf} [37–42], with particles of group B or group A (e.g. sand, SiC, TiO_2, Ni, etc.). Llop *et al.* [43] point out that, at low pressure, the hydrodynamic flow regime is no longer laminar and is better described with the assumption of a slip-flow effect. Under these conditions, the hydrodynamic behavior deviates from what is observed at atmospheric pressure. Zarekar *et al.* [42] propose to modify the correlations proposed by Richardson and Llop [44,43] by including the contribution of the rarefied flow. These correlations consider the slip-flow effect through the Knudsen number ($Kn = {\lambda}/{d_p}$), i.e. the ratio of the mean free path of the gas molecules (λ) to the characteristic length of the flow, here considered as the pore diameter (d_p) created by the granular load. Zarekar *et al.* [42] thus demonstrate the dependence of the particle Reynolds number at minimum fluidization velocity ($Re_{mf} = {U_{mf}\rho_g d_g}/{\mu}$), to the Archimedes number ($Ar = {g(\rho_p - \rho_g)\rho_g d_g^3}/{\mu^2}$), the particle sphericity (ψ_s) and the Knudsen number (Equation 1):

$$Re_{mf} = -\frac{25.7}{\psi_s(1+8.8Kn)} + \sqrt{\left(\frac{25.7}{\psi_s(1+8.8Kn)}\right)^2 + 0.0365\psi_s Ar} \qquad \textit{Equation 1}$$

The authors predict a critical pressure for which the rarefied flow accounts for at least 10% of the total flow at around 104 mbar for particle diameter of 213 µm, fluidized in air at 20°C.

2.2. Influence of the temperature

Few experimental studies have been dedicated to the temperature dependence of the minimum fluidization velocity. Moreover, when the study is carried out, it is often at temperatures that rarely exceed 700°C. From a theoretical point of view, the temperature is involved in the density of the carrier gas ($\rho_g \propto {1}/{T}$), the viscosity ($\mu \propto T^n$ with $n = 0.5$ to 1) and the gas mean free path ($\lambda \propto \sqrt{T}$). Thus, as the temperature increases, the density decreases, the viscosity and the mean free path increase. The direct link to the minimum fluidization velocity U_{mf} is non-trivial and depends on the size of the fluidized particles. A wide variety of particles have been studied: of different nature (ilmenite, sand, limestone, quartz, ...), and Geldart category (A, B and C) [45–48]. For the particles of interest here (e.g. particles of groups A and B), the authors distinguish two distinct behaviors:

- Group A particles: for which U_{mf} decreases as T increases
- Group B particles: for which U_{mf} increases with T at low temperature and decreases at higher temperature.

At atmospheric pressure, Shao *et al.* [47] show that for a given particle density and for different particle sizes, the variation of U_{mf} is more or less significant. Smaller particles cause very little variation of U_{mf} as a function of temperature, while larger particles show steeper curves of minimum fluidization velocity as a function of temperature. This behavior is explained by the lower drag force created by larger particles which involves the need of higher superficial gas velocity for the flow to occur. In the case of smaller particles, the large contact areas involve lower superficial gas velocity for the flow.

One of the main difficulties in using high temperature correlations is the measurement of the bed porosity at the minimum fluidization velocity. This value is difficult to measure since, most of the time, the fluidized bed is hidden by heating elements. Botterill *et al.* [49] draw attention to hazardous generalized predictions based on tests carried out under ambient conditions. They measured the porosity of a sand bed ($d_g = 775$ µm) as a function of

temperature and noticed that it varied with temperature. This porosity decreases from ambient to 170°C from 0.422 to 0.408 and increases up to 0.432 at 860°C. Saxena and Grewal [50] replied to Botterill *et al.* that the method of bed porosity measurement does not permit an accurate assessment of the uncertainty of the average bed porosity at minimum fluidization velocity. A dispersion of the measurements over only 6% does not allow to claim a temperature dependence of the bed porosity on the minimum fluidization velocity, especially as there is no physical explanation for this variation of the porosity as a function of the bed temperature. For smaller sand particles ($d_g = 100\ \mu m$) Raso *et al.* [51] highlighted the potential impact of interparticle forces on bed porosity at minimum fluidization velocity, as a function of temperature. Indeed, as the temperature increases, the interparticle forces become stronger (especially for small diameter particles where the Van der Waals forces are not negligible) and the porosity of the bed increases with temperature up to more than 25%.

It should be mentioned that the experimental assessment and interpretation of the pressure drop changes as a function of the gas velocity are extremely delicate. Indeed, at high temperature, in the fixed bed zone, the thermal homogeneity is very sensitive to the gas velocity. If the thermal distribution is altered, the determination of the pressure drop is subject to significant errors.

2.3. Bed expansion

Bed expansion varies in a complex way depending on the hydrodynamic properties of the particle load. The initial bed height, particle density, viscosity and gas density are among the parameters that drive the propensity of the load to expand more or less. The proposed correlations are based on the two-phase theory [52,53] and/or bubble growth [54–57]. In general, there is no single model for the expansion of fluidized beds; each author proposes a correlation specific to his own particular conditions (cf. Table 1). All models can be reduced to a single formula, the parameters of which differ between authors:

$$\frac{H}{H_{mf}} = 1 + \alpha(U - U_{mf})^{n_1} U_{mf}^{n_2} \rho_p^{n_3} \rho_g^{n_4} d_g^{n_5} \qquad \textit{Equation 2}$$

Table 1 : Correlations of bed expansions proposed by the literature

Authors	Parameters						Conditions		
	α	n_1	n_2	n_3	n_4	n_5	Parameter	Min	Max
Chitester *et al.* [35]	1.957	0.738	-0.937	0.376	-0.126	1.006	H/H_{mf} P (bar) d_g (µm) ρ_p (kg.m^{-3})	1 1 102 1116	1.1 63 361 2472
Feng *et al.* [58]	2.58	0.2014	0.154	0	0.0846	-0.1004	H/H_{mf} P (bar) d_g (µm) ρ_p (kg.m^{-3})	1 1 550 1020	2.4 25 1340 1020
Lewis *et al.* [59]	0.0188	1	0	0	0	-0.5	H/H_{mf} P (bar) d_g (µm) ρ_p (kg.m^{-3})	1 0.008 100 2355	1.9 0.12 600 2483
Rashid *et al.* [60]	20	0.716	-0.937	0.376	-0.126	1.006	H/H_{mf} P (bar) d_g (µm) ρ_p (kg.m^{-3})	1 0.1 275 2500	1.7 0.1 275 2500

Despite the discrepancies noted between each author, all of them agree that H/H_{mf} varies as a function of $(U - U_{mf})^{n_1}$ with $n_1 > 0$. For the exponents n_i, i = 2 to 5 of the other parameters (U_{mf}, ρ_p, ρ_g, d_g respectively), there is no clearly identified general trend.

2.4. Theoretical aspects of hydrodynamic laws

Many hydrodynamic laws are available to predict the characteristics of the flow through a granular medium. Among them, the Ergün's law is considered as a reference and others, like that proposed by Zarekar *et al.*, adjust coefficients to account for particular flows (e.g. rarefied, in the latter case). The current study investigates the validity of these equations in the particular case of a fluidized bed CVD reactor, applied to a substrate that is also specific: SiC short fibers and powders. This section introduces the hydrodynamic basis of the Ergün's equation and develops the fundamental equation of a Darcy-Klinkenberg flow, adapted to the case of a granular porous medium. These equations will be used as a basis for the adjustment of the experimental data to deduce intrinsic information on the various granular media.

Very often, the effect of the pressure/temperature parameters are described through the Ergün equation [31]:

$$\frac{\Delta P_{bed}}{H} = 150\frac{(1-\varepsilon)^2}{\varepsilon^3}\frac{\mu U}{(\psi_s d_g)^2} + 1{,}75\frac{(1-\varepsilon)}{\varepsilon^3}\frac{\rho_g U^2}{(\psi_s d_g)} \qquad \textit{Equation 3}$$

Through a balance of forces at the minimum of fluidization and by introducing the Archimedes and Reynolds numbers taken in the conditions of the minimum of fluidization, the Ergün equation leads to:

$$Re_{mf} = (A^2 + B\,Ar)^{\frac{1}{2}} - A \qquad \textit{Equation 4}$$

Either:

$$U_{mf} = \frac{\mu}{\rho_g d_g}\left[(A^2 + B\,Ar)^{\frac{1}{2}} - A\right] \qquad \textit{Equation 5}$$

Where $A = K_2/2K_1$; $B = 1/K_1$; $K_1 = 1.75/\varepsilon_{mf}^3\psi_s$ and $K_2 = 150(1-\varepsilon_{mf})/\varepsilon_{mf}^3\psi_s^2$

Since our study is carried out below atmospheric pressure, it is necessary to consider another type of flow, which is negligible at pressures above atmospheric pressure. In fact, the Ergün equation is based on the combined effect of laminar and inertial flows. These conditions are verified in most fluidization studies. However, in our study, the flow tends to be more laminar than inertial, and even, at reduced pressure, rarefied. In the case of negligible inertial effects (Reynolds number: $Re = U\rho_g d_p/\mu < 1$) and a Knudsen diffusion contribution ("slip-flow" effect at Knudsen number: $Kn = \lambda/d_p < 10^{-2}$), the Ergün equation is no longer adapted. Therefore, we prefer to use Darcy's law corrected by Klinkenberg [61], which takes the rarefaction of the carrier gas into account. Written as a function of the mass flux, and using the law of perfect gases we have:

$$j = \frac{M}{\mathcal{R}T}\underbrace{\left(\frac{P}{\mu}K + D_K\right)}_{K_{app}}\frac{\Delta P_{bed}}{H} \qquad \textit{Equation 6}$$

In this expression appear the permeability coefficient K, specific to viscous laminar (Darcy) flows and the Knudsen diffusivity coefficient D_K, specific to rarefied flows (both values are gathered in the global coefficient K_{app}). These two coefficients are related to the equivalent pore diameter (d_p) and respectively the viscous and Knudsen tortuosities (η_v and η_K) by the following relations:

$$K = \varepsilon \eta_v^{-1} \frac{d_p^2}{32} \quad \textit{Equation 7}$$

$$D_k = \varepsilon \eta_K^{-1} \frac{1}{3} c d_p \quad \textit{Equation 8}$$

With $c = \sqrt{\frac{8\mathcal{R}T}{\pi M}}$ the molecular velocity. Integrating Equation 6 between the pressures at the inlet (P^+) and outlet of the bed (P^-) we have:

$$\int_{P^-}^{P^+} j = \frac{M}{\mathcal{R}T} \int_{P^-}^{P^+} \left(\frac{K}{\mu} P + D_K\right) \frac{dP}{H} = \frac{M}{H\mathcal{R}T} \left[\frac{K}{\mu}\left(\frac{P^2}{2}\right) + D_K P\right]_{P^-}^{P^+} \quad \textit{Equation 9}$$

$$\frac{Q}{S} = \frac{M}{H\mathcal{R}T} \left[\frac{K}{\mu}\left(\frac{P^{+2} - P^{-2}}{2}\right) + D_K (P^+ - P^-)\right] \quad \textit{Equation 10}$$

Yet $\frac{P^{+2} - P^{-2}}{2} = \Delta P_{bed} \left(\frac{\Delta P_{bed}}{2} + P^-\right) = \Delta P_{bed} \times P_{mean}$, which leads to:

$$\frac{Q}{S \Delta P_{bed}} = \frac{M}{H\mathcal{R}T} \left(\frac{P_{mean}}{\mu} K + D_K\right) \quad \textit{Equation 11}$$

From the coefficients K and D_K it is therefore possible to:

- Either determine the equivalent pore diameter (d_p) representative of the fluidized bed from Equations 7 and 8, assuming the tortuosity values (η_v and η_K) :

$$d_p = \sqrt{\frac{32K}{\eta_v \varepsilon}} \quad \textit{Equation 12}$$

$$d_p = \frac{3 D_K \eta_K}{\varepsilon} \sqrt{\frac{\pi M}{8\mathcal{R}T}} \quad \textit{Equation 13}$$

- Or determine the tortuosity values (η_v and η_K) from the pore diameter (d_p).

$$\eta_v = \frac{32K}{d_p^2 \varepsilon} \quad \textit{Equation 14}$$

$$\eta_K = \frac{\varepsilon d_p}{3 D_K} \sqrt{\frac{8\mathcal{R}T}{\pi M}} \quad \textit{Equation 15}$$

One of the difficulties in the viscous flow through porous media is that the characteristic length is the pore diameter (d_p), while the size often available in particulate or fibrous media is the diameter of the particles (d_g). Kozeny and Carman [62] developed an expression where the quantity involved is the internal surface area S_v :

$$K = \frac{\varepsilon^3}{K_{KC} S_v^2} \quad \textit{Equation 16}$$

where the constant K_{KC} depends on the family of the porous medium studied and is equal to twice the viscous tortuosity. The internal surface area is equal to the specific surface area S_s (in m^2 of surface area per m^3 of solid volume) of the porous medium multiplied by the solid volume fraction (ϕ): $S_v = \phi S_s$. The internal surface area can be related to the hydraulic diameter of the pores [63] :

$$S_v = \frac{4\varepsilon}{d_p} \qquad \textit{Equation 17}$$

Then, comes the Kozeny-Carman relationship as a function of pore (d_p) or particle (d_g) diameter:

$$K = \varepsilon \frac{d_p^2}{32\eta_v} = \frac{\varepsilon^3}{(1-\varepsilon)^2} \frac{d_g^2}{32\eta_v} \qquad \textit{Equation 18}$$

Given the relationship between the pore diameter (d_p) and the particle diameter (d_g):

$$d_p = \frac{\varepsilon}{(1-\varepsilon)} d_g \qquad \textit{Equation 19}$$

From Equations 7, 8, 11 and 19, comes:

$$U = \frac{\Delta P_{bed}}{H} \frac{P^0 M}{T^0 \mathcal{R}} \left[\frac{1}{32\eta_v} \frac{\varepsilon^3}{(1-\varepsilon)^2} \frac{d_g^2}{\mu} + \frac{1}{3\eta_K} \frac{\varepsilon^2}{(1-\varepsilon)} \frac{c d_g}{P_{mean}} \right] \qquad \textit{Equation 20}$$

U is thus dependent on the temperature only via the reciprocal viscosity of the carrier gas (itself proportional to $T^{0.8}$ in the case of nitrogen) and c (proportional to $T^{0.5}$). Using, like Ergün, the balance of forces, we have:

$$\Delta P_{bed} S = S H_{mf} (1-\varepsilon_{mf})(\rho_p - \rho_g) g \qquad \textit{Equation 21}$$

The expression of U_{mf} at the minimum fluidization velocity conditions is deduced:

$$U_{mf} = \frac{P^0 M}{T^0 \mathcal{R}} (\rho_p - \rho_g) g \left[\frac{1}{32\eta_v} \frac{\varepsilon_{mf}^3}{(1-\varepsilon_{mf})} \frac{d_g^2}{\mu} + \frac{1}{3\eta_K} \varepsilon_{mf}^2 \frac{c d_g}{P_{mean}} \right] \qquad \textit{Equation 22}$$

Or, written in terms of K and D_k coefficients:

$$U_{mf} = \frac{P^0 M}{T^0 \mathcal{R}} (\rho_p - \rho_g) g (1-\varepsilon_{mf}) \left[\frac{K}{\mu} + \frac{D_K}{P_{mean}} \right] \qquad \textit{Equation 23}$$

Equation 6 leads, by combining Equations 7, 8 and 19, to a generalized Darcy relation where an apparent permeability K_{app} appears, which is a function of the particle diameter (d_g), the viscous and Knudsen tortuosities (η_v and η_K), pressure (P), and molecular velocity (c):

$$K_{app} = \frac{\varepsilon^2 d_g}{(1-\varepsilon)} \left[\frac{\varepsilon P d_g}{32\eta_v (1-\varepsilon)\mu} + \frac{c}{3\eta_K} \right] \qquad \textit{Equation 24}$$

Figure 1 shows the weight of the laminar/inertial relative contributions in the Ergün equation (cf. Equation 3) and laminar/rarefied effects in Equation 22, at room temperature, and in the range of pressures explored (cf. Equation 24). Considering the Ergün equation, the inertial flow represents at most 8% at room temperature and atmospheric pressure. At reduced pressure, in the range of gas velocities necessary for the fluidization of short fiber/powder mixtures, rarefied flow can't be neglected, unlike inertial flow. Indeed, at 200 mbar and depending on the temperature, the contribution of the inertial flow is negligible (cf. Figure 1).

Although Equation 22 may seem similar to that proposed by Zarekar *et al.* [42], it is different by i) the assumption of a totally negligible inertial flow and ii) the use of tortuosity features rather than sphericity. A critical pressure can be evidenced, for which the rarefied flow accounts for at least 10% of the overall flow around 115 mbar, for particles of a diameter of 213 µm, fluidized in air at 20°C ($\varepsilon = 0.4$, $\eta_v = 8$ and $\eta_K = 4$), i.e. a value comparable to that predicted by Zarekar *et al.* With a particle diameter of 70 µm, fluidized in nitrogen at 20°C ($\varepsilon = 0.4$, $\eta_v = 8$ and $\eta_K = 4$), the rarefied flow accounts for at least 10% of the total flow when the pressure is below 340 mbar.

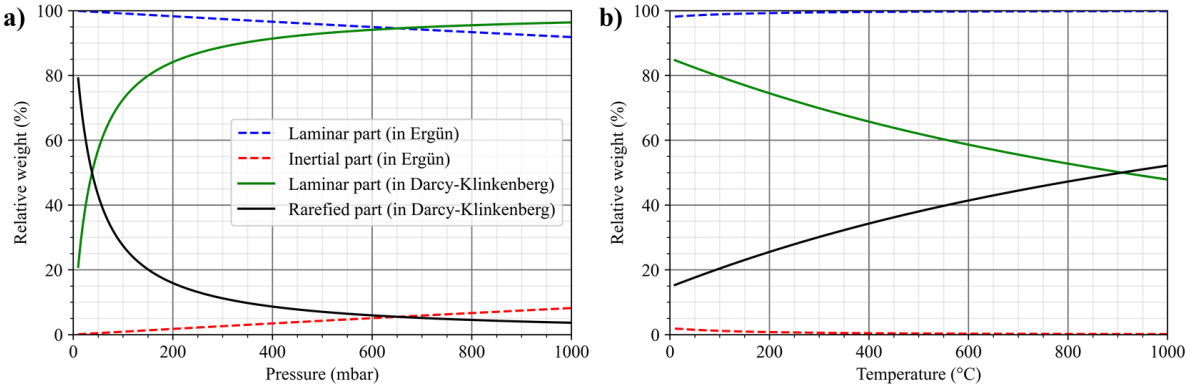

Figure 1 : Contribution of the coefficients of laminar/inertial flow in the Ergün equation and laminar/rarefied flow in the Darcy-Klinkenberg equation. According to a) the pressure at 20°C and according to b) the temperature at 200 mbar (calculated with $\varepsilon = 0.5$; $d_g = 60\mu m$; $\eta_v = 6$ *and* $\eta_K = 2$*)*

Figure 2 compares the prediction of U_{mf} as a function of temperature and pressure from Equations 3 and 22, as well as the relative error made when considering the Ergün equation instead of Equation 22. It is clear that, at low pressures, the contribution of the rarefied flow is significant and can't be neglected. The temperature effect on the rarefied flow is obvious: it becomes increasingly significant as the temperature rises and this, even at atmospheric pressure.

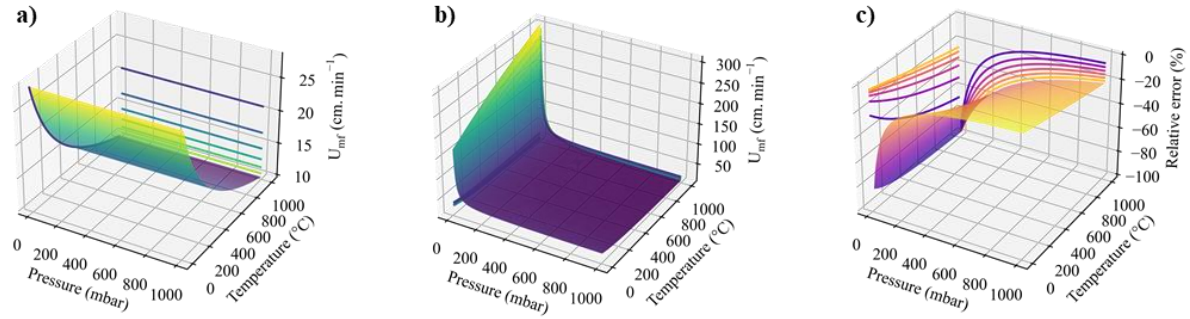

Figure 2 : Comparison of U_{mf} *as predicted from the a) Ergün and b) Darcy-Klinkenberg equations, and c) relative error mapping. (calculated with* $\rho_p = 3210\ kg.m^{-3}$; $d_g = 60\ \mu m$; $\varepsilon_{mf} = 0,4$; $\psi_s = 1$; $\eta_v = 6$ *and* $\eta_k = 2$*)*

2.5. Materials

The fluidization behavior of the short fiber/powder mixture was analyzed at different pressures ranging from 10 to 800 mbar and different temperatures up to 1000°C. The powder used consists of α silicon carbide (FEPA 220 from LAM PLAN). The short SiC fibers were produced by milling long Hi-Nicalon type S fibers (from NGS Advanced Fibers Co., Ltd.). The milling process produces short fibers with a wide length dispersion (20-1000 µm)

centered around 150 µm and diameters ranging from 12 to 25 µm (cf. Figure 3). The powder was submitted to grain size analysis using laser diffraction (Fritsch Analysette 22 nanotec) and the dimensions of the fibers were determined by image analysis (Malvern Instrument Morphologi G3S). The powder meeting the Fraunhofer conditions, the laser diffraction analysis can be considered as valid. The short fibers were dry dispersed before microscopic image acquisition and processing, to provide the fiber length and diameter distributions. A population of fiber fragments appears on the particle size distribution results on both fiber diameter (between 20 and 30 µm) and length (between 30 and 50 µm). The particle size distribution of the SiC powder was narrowed by sieving, resulting in a 30-150 µm range centered at 70 µm. (cf. Figure 3). The properties of the short fibers and the powder are presented in Table 2. In order to ensure a good homogeneity, the short fibers and the powder were mixed directly in the fluidized bed at a velocity well above U_{mf} for several minutes.

Table 2 : Properties of short fibers and SiC powder.

		Short fibers	SiC powder
Geometry	Shape	Cylindrical	Near-spherical
	Sphericity *as defined by [64]*	~ 0.67	~ 0.9
	Form factor	~ 10	~ 1
Length	L_{min} (µm)	24.41	NA
	L_{mean} (µm)	152.20	NA
	L_{max} (µm)	2271.60	NA
	L_{10} (µm)	44.27	NA
	L_{50} (µm)	118.91	NA
	L_{90} (µm)	293.68	NA
	$L_{3,2}$ (µm)	388.00	NA
Diameter	D_{min} (µm)	7.34	24.1
	D_{mean} (µm)	17.64	75.4
	D_{max} (µm)	92.84	186
	D_{10} (µm)	13.87	47.1
	D_{50} (µm)	15.86	76.2
	D_{90} (µm)	24.11	120
	$D_{3,2}$ (µm)	21.21	71.0
Specific surface	S_S ($\times 10^{-2}$ $m^2.g^{-1}$)	8.25 ± 0.04	3.62 ± 0.02
Density	ρ_{tapped} ($g.cm^{-3}$)	0.866 ± 0.006	1.773 ± 0.013
	ρ_{bulk} ($g.cm^{-3}$)	0.584 ± 0.003	1.642 ± 0.007
Flowability	Hausner ratio	1.482 ± 0.014	1.079 ± 0.008

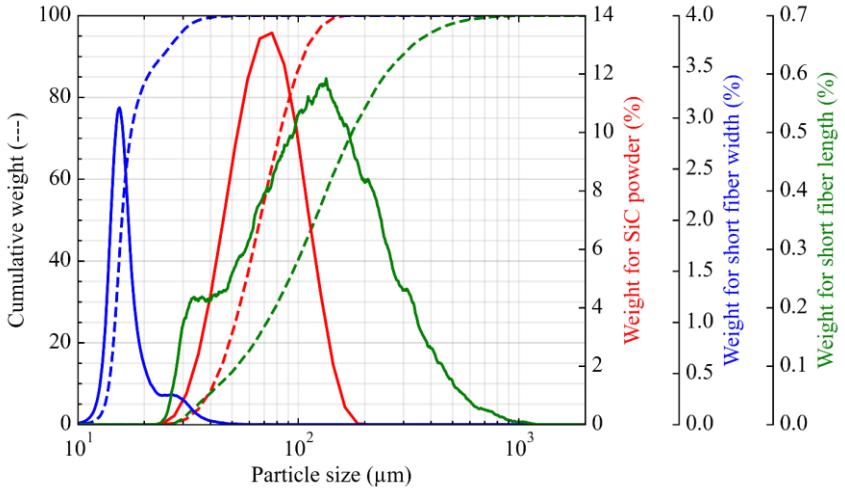

275

Figure 3 : Particle sizes distributions of short fibers lengths, diameters and SiC powder diameters.

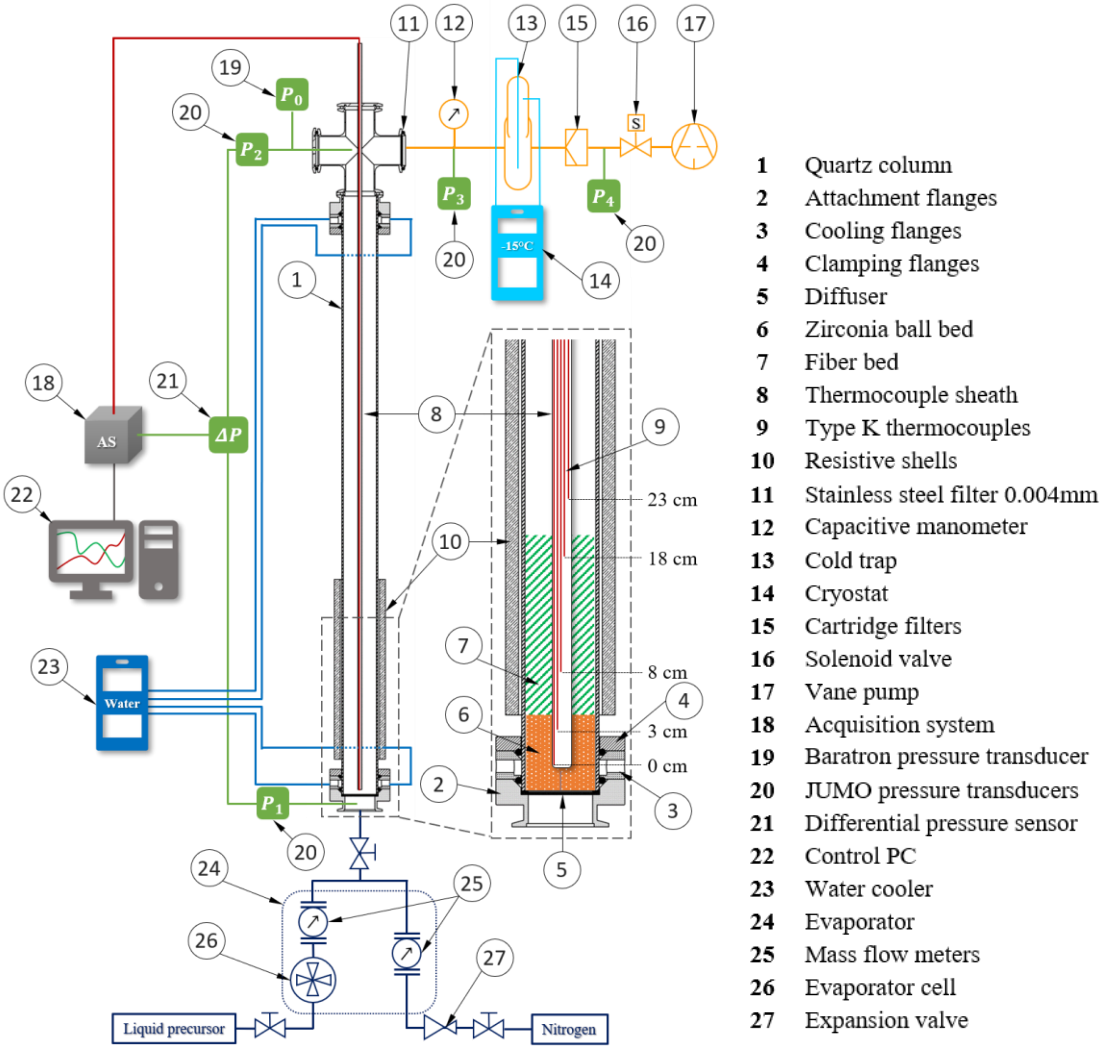

Figure 4 : Schematic of the fluidized bed CVD reactor.

A scheme of the experimental setup is shown in Figure 4. The fluidization column is a silica glass tube (1) with
280 an internal diameter of 55 mm and a total length of 1000 mm. At the base of the column, a succession of attachment

(2), cooling (3) and clamping (4) flanges host a PORAL® microporous stainless-steel distributor, 60 mm in diameter and 2 mm in thickness (5). The permeability of the gas distributor (given by the supplier) is between 0.6 and 1.2 Darcy. The carrier gas (nitrogen) supply is ensured by a commercial evaporator CEM LAB from 2M PROCESS (24). This device allows the mixing of a carrier gas and the CVD precursor, which is previously evaporated from the liquid phase; for the needs of the study, only the carrier gas is used. The nitrogen flow rate is measured with an EL-FLOW Select mass flow meter from Bronkhorst, installed in the evaporator. At the top (outlet) of the system, a second set of flanges ensures the sealing of the fluidization column. The gas evacuation is ensured by an Alcatel Adixen 2021 C2 vane pump (17) equipped at the entrance with a HEPA NW25 particle filter (15) and a 4 µm stainless steel filter (11). The fluidization system is able to operate at reduced pressure. Several pressure measurements are taken at different relevant locations: under the diffuser (P1), at the top of the fluidization column (P2), between the grid and particle filters (P3) and just before the pump (P4). Each of these pressures is measured by a JUMO dTRANS p30 sensor. The total pressure of the fluidizing reactor is measured at the same level as P2 with an MKS Baratron Type 627D pressure sensor (P0). A motorized valve MKS Type 253B (16) placed at the pump inlet and controlled by a pressure regulator MKS 600 series 651CD regulates the pressure in the column. The pressure drop between the top and the bottom of the fluidized bed (eg P1-P2) is acquired through a MKS series 660 display. A stainless-steel rod (8) containing five type K (Ni-Cr) thermocouples placed at different heights is installed in the center of the column to acquire the temperature at several levels along the longitudinal axis of the bed. Two resistive heating shells (10) can be positioned on both side of the silica tube. The bed is raised to the center of the heating shells by the addition small zirconia balls (6) [65]. The zirconia balls bed serves as thermal insulator to protect the gas distributor and the Viton seals from overheating. It acts as a second-high permeability porous medium, in series between the stainless-steel distributor and the fluidized bed.

For each fluidization run, a load of zirconia balls is first placed in the fluidization column. This first layer has the function of thermally protecting the flange elements during the CVD deposition which often requires high temperatures (>800°C). The ZrO_2 spheres used are sufficiently dense and large (5.68 $g.cm^{-3}$ and 500 µm in diameter) to remain fully static under the gas flow, within the gas velocity, pressure and temperature ranges used. Furthermore, their arrangement is sufficient compact to prevent the load from leaking through. A 400 g mass of a short fiber/powder mixture is then poured on top of the balls, from upper entrance of the fluidization column. The height of the SiC particle mixture thus reaches approximately 15.5 cm, corresponding to a height/diameter ratio of 2.8. A ruler is placed on the glass column to measure (at room temperature only) the approximate height of the expanded bed. The tests at different pressures were conducted at room temperature (25°C). The set point and PID parameters are adjusted to reach the desired pressure (800, 600, 400, 200, 100, 50, 25 and 10 mbar). For the experiments at different temperatures, the pressure is fixed at 200 mbar. The heating shells are then placed on both sides of the tube with insulating elements at the top and bottom of the shells, to maintain a homogeneous temperature along the bed and avoid overheating the rest of the system.

The hydrodynamic parameters of the fluidized bed are processed by a semi-automated calculation code that determines the minimum fluidization velocity U_{mf} (by the method of Davidson and Harrison [66]) the linear pressure drop of the diffuser/ball bed and ΔP_{∞}^{*} [67], i.e. the normalized pressure drop plateau at high velocity of the $\Delta P^{*}(U)$ curves, which reflects whether the whole bed is supported by the carrier gas (i.e. $\Delta P_{\infty}^{*} = 1$) or not (i.e. $\Delta P_{\infty}^{*} < 1$). The latter value can therefore be considered as a quality factor for fluidization. Indeed, when ΔP_{∞}^{*} is

lower than 1, the experimental pressure drop of the bed (ΔP_{bed}) is lower than the one expected theoretically ($\Delta P_{theoretical}$). In this case, there are preferential gas channels within the bed and only a fraction of the total load is fluidized. These conditions are unfavorable to consider any coating deposition.

The bed pressure drop (ΔP_{bed}) is normalized by the theoretical pressure drop ($\Delta P_{theoretical}$):

$$\Delta P^* = \frac{\Delta P_{bed}}{\Delta P_{theoretical}} = \frac{\Delta P_{bed}}{mg/S} \qquad \textit{Equation 25}$$

Where m is the mass of the bed, g is the gravitational constant and S is the cross section of the column. The bed expansion, measured at room temperature, is normalized by the bed expansion at minimum fluidization velocity (H_{mf}) to obtained H^*, such that:

$$H^* = \frac{H}{H_{mf}} \qquad \textit{Equation 26}$$

Where H is the bed height and H_{mf} is the bed height at the minimum fluidization velocity. These heights are measured with less than 10% uncertainties.

3. Results

3.1. Short fibers and powder fluidization

The short fibers can't be included in the Geldart classification, which predicts the fluidization tendency of a powder according to its density and particle diameter. A hydrodynamic study was conducted to understand the fluidization behavior of this new substrate. It explores the hydrodynamic properties according to two main parameters: the temperature within the bed and the pressure in the reactor chamber. The study compares two types of loads: short fiber/powder mixtures and powder alone.

The ratio between the tapped and bulk density of particulate materials, known as the Hausner index $HR = \rho_{tapped}/\rho_{bulk}$. [68], provides interesting information on the fluidization behavior of powder. Thus, empirically, it is considered that for ratios higher than 1.35, fluidization is not possible since the forces between the particles prevent suspension [69,70]. The Hausner ratio was determined as a function of different short fiber/powder volume fractions (cf. Figure 5) under ambient temperature and pressure conditions. The Hausner ratios corresponding to each mixture were plotted as a function of: i) the mass ratio, calculated from the true densities of the short fibers and powders, ii) the aerated volume ratio between the short fibers and powders calculated from the aerated densities of the two materials, and iii) the tapped ratio between the short fibers and the powders calculated from the tapped densities of the two materials. The Hausner ratio varies linearly with the volume fraction calculated from the tapped density. The corresponding linear regression is plotted in Figure 5.

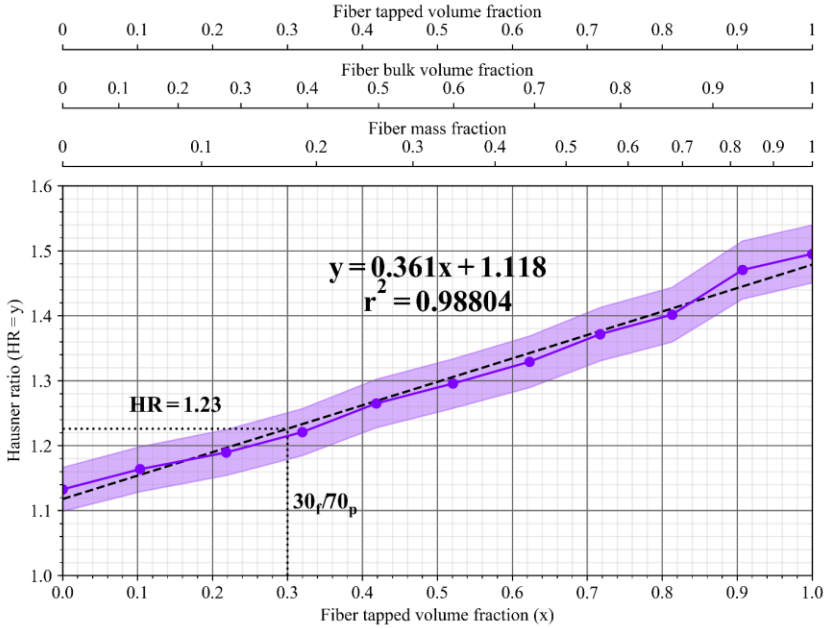

Figure 5 : Hausner ratio as a function of the short fibers tapped volume ratio of short fiber/powder mixtures (the mass and aerated short fibers volume ratios corresponding to the short fibers tapped volume ratio are shown above).

Figure 5 clearly shows that the short fibers alone do not exhibit a satisfactory flowability to be fluidized on their own due to a Hausner ratio of 1.482 ± 0.014. On the contrary, the powder appears easily fluidizable according to Hausner's criterion, with a Hausner ratio of 1.079 ± 0.008, but also according to Geldart's classification, since it belongs to the B category. To confirm these predictions, two different beds of pure short fibers and pure powder were placed in the fluidization column and tested separately. The powder bed was indeed easy to fluidize whereas the short fibers bed fluidization behavior was erratic and irreproducible. The bed of short fibers started to move at the beginning of the gas injection, but quickly settled down by creating preferential paths for the gas to pass through (channeling effect). The images shown in the supplementary material illustrate the typical behavior of a bed consisting only of short fibers. According to Figure 5, a mixture consisting of 30% tapped volume of short fibers and 70% tapped volume of powder (namely: $30_f/70_p$) has a sufficient flowability to predict a correct fluidization. As a matter of fact, with the $30_f/70_p$ mixture, the different regimes expected during proper fluidization were observed successively with increasing gas velocity: fixed bed, minimum fluidization velocity, bubbling bed and turbulent bed, all being indicators of a correct fluidization behavior. Hence, the $30_f/70_p$ mixture was considered for the rest of the study on the fluidization parameters.

3.2. Experimental results

3.2.1. Pressure effect

In order to compare the contribution of short fibers in the particulate mixtures subjected to fluidization, the behavior of the pure powder was first examined. A powder bed was fluidized at different pressures (800, 600, 400, 200, 100, 50, 25 and 10 mbar). The experiments were performed at room temperature (25°C), the removal of the heating shells allowing a direct observation of the fluidization process. The results are presented in Figure 6.

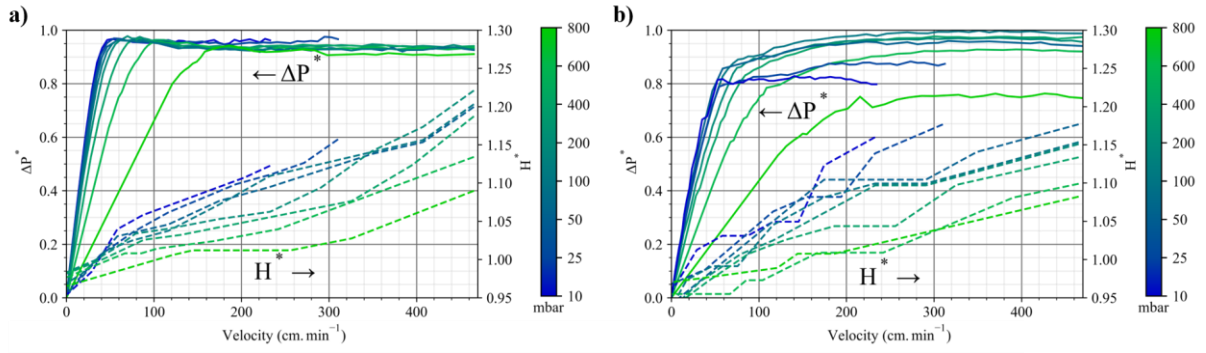

370 ***Figure 6 : Normalized pressure drop (ΔP^* in solid lines) and normalized expansion (H^* in dashed lines) of a) the pure SiC powder bed and b) $30_f/70_p$ mixture, as a function of pressure and gas velocity.***

For the pure powder (cf. Figure 6.a), the pressure drop curves are classical compared to those reported in literature. The curves exhibit a first linear part at low velocities and a plateau at higher velocities. All curves tend to a normalized pressure drop close to 1 and the slopes of the linear parts decrease as the pressure decreases. The bed
375 expansions evolve linearly and their slopes increase as pressure increases.

For the short fiber/powder mixture (cf. Figure 6.b), the pressure drop curves are clearly less resolved than those for the pure powder. Some curves deviate from an asymptotic value close to 1; for example, at 10 mbar the curve tends towards $\Delta P^*_\infty = 0.78$. Nevertheless, there is some curves between 25 and 600 mbar for which ΔP^*_∞ is close to 1. The bed expansions evolve linearly with a slope that increases as the pressure increases.

380 ### 3.2.1. Temperature effect

A study of the influence of temperature on the minimum fluidization velocity was conducted on a pure powder bed, in a similar way to that conducted as a function of pressure. The pressure was set at a constant value of 200 mbar and the temperature gradually raised from ambient to 1000°C (25, 200, 400, 600, 800 and 1000°C). The bed porosity at minimum fluidization velocity was assumed to be identical, at all temperatures, to that observed at
385 room temperature. The results are shown in Figure 7. The determination of the pressure drop in the fixed bed area is difficult to carry out while maintaining a good thermal homogeneity throughout the bed. In order to approach as closely as possible the pressure drop values in this zone, the gas velocity is increased beyond U_{mf}, maintained for a few minutes to recover a good thermal homogeneity and then rapidly reduced. The retained pressure drop corresponds to the value reached after stabilization over a few minutes.

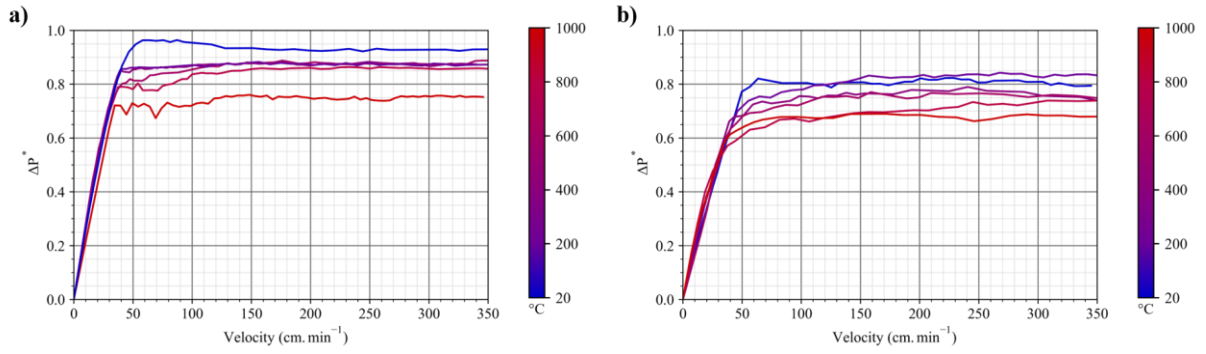

390

Figure 7 : Normalized pressure drop (ΔP^* in solid lines) of a) the pure SiC powder bed and b) $30_f/70_p$ mixture, as a function of temperature and gas velocity.

For the pure powder (cf. Figure 7.a), the pressure drop curves are again classical compared to those reported in literature. However, there is a marked difference for ΔP_∞^* as a function of temperature, ΔP_∞^* starts at 0.94 at room temperature and drops to 0.75 at 1000°C. The first linear part seems to be not sensitive to the temperature variation.

For the short fiber/powder mixture (cf. Figure 7.b), the pressure drop vs. carrier gas velocity curves show the same tendency as those observed as a function of the pressure. Again, ΔP_∞^* varies with temperature from 0.82 at room temperature to 0.69 at a minimum at 1000°C. The transition from the fixed bed to the fully supported bed is slow and progressive. The first linear part of the curves seems to be slightly more sensitive to the temperature than those observed for the powder.

4. Discussion

4.1. Effect of pressure

4.1.1. Powder

The normalized pressure drops (cf. Figure 6.a) generated by the powder bed (ΔP^*) are very sensitive to the total pressure in the reactor, especially on the first linear part of the curves, when the powder bed is fixed. A decrease in the slope of the initial linear part is observed as the pressure decreases in the reactor, resulting in an increase in the minimum fluidization velocity. At the same time, the normalized expansion (H^*) increases with the pressure at constant gas velocity. This is expected by the two-phase theory which predicts that the excess velocity ($U - U_{mf}$) feeds the bubble phase which increases the bed expansion.

The minimum fluidization velocities of the powder alone are extracted and plotted as a function of pressure in Figure 8.a. The powder's minimum fluidization velocity increases as the pressure decreases. From 800 mbar down to 100 mbar, U_{mf} varies only slightly (from 32 cm.min^{-1} to 40 cm.min^{-1}) while below 100 mbar, U_{mf} increases very rapidly, reaching 138 cm.min^{-1} at 10 mbar. The fluidization quality factor, ΔP_∞^*, is not very dependent on the pressure in the reactor (cf. Figure 8.b): it remains around 0.95 for the whole studied range of pressure suggesting that fluidization is well maintained at all pressures.

From the Ergün equation (cf. Equation 5) and the correlation of Zarekar *et al.* (cf. Equation 1), by fitting the equations to the experimental data, comes an effective particle diameter of $\psi_s d_g = 66.9 \pm 2.8$ µm and $\psi_s d_g = 67.6 \pm 1.2$ µm, respectively. 2D image analyses were carried out to better evaluate the powder sphericity. The average value obtained is close to 0.9 leading to a particle diameter d_g between 71.2 µm and 77.4 µm, which is close to the powder mean diameter measured by laser diffraction ($d_g = 75.4$ µm). The resulting fitted equations are plotted in Figure 8.a in function of the pressure. These equations correlate well with the experimental data from atmospheric pressures to 200 mbar, but does not accurately reproduce the experimental behavior under 100 mbar. The Ergün equation leads to a mean relative error of 24%, with a maximum relative error of 74% at 10 mbar, whereas the correlation of Zarekar *et al.* leads to a mean relative error of 13%, with a maximum relative error of 43% at 10 mbar. This last equation nevertheless describes the increasing tendency of U_{mf} below 200 mbar.

The permeability (K) and Knudsen coefficients (D_k) can be determined from the linear correlation of $\frac{Q}{S\Delta P}$ as a function of P_{mean} (cf. Equation 11): $K = 4.05.10^{-12} \pm 3.29.10^{-14}$ m^2 and $D_K = 7.13.10^{-4} \pm 2.03.10^{-5}$ m^{2}s^{-1}. From these coefficients, it is possible to determine, via the Kozeny-Carman equation (cf. Equations 18 and 19) either: the viscous and Knudsen tortuosities (η_v and η_k) at a given particle diameter (d_g), or, the reciprocal: the particle diameter (d_g) at given viscous and Knudsen tortuosities (η_v and η_k). Here, starting from the properties of the powder bed ($d_g = 71$ µm, $\varepsilon_{mf} = 0.4$), both tortuosity values were evaluated: $\eta_v = 7.52 \pm 0.06$ and $\eta_K = 4.42 \pm 0.13$, respectively. These values are consistent with the geometry and fluidization behavior of the powder. The fitted equation is plotted in Figure 8.a in function of the pressure. The correlation is in good agreement with the experimental data and allows predicting U_{mf} with a mean relative error of 2% and a maximum relative error of 5% at 10 mbar.

4.1.2. Short fiber/powder mixture

As for the pure powder, the short fiber/powder mixture shows a fluidization behavior that depends on the working pressure. The pressure drop curves are much less resolved than those for the powder, but all remain characteristic of a correct fluidization process (cf. Figure 6.b). As for the powder, the slope of the first linear part of the pressure drop curves decreases as the pressure decreases but ΔP_∞^* varies with the pressure without showing a general monotonic behavior. The normalized expansion (H^*) increases with the pressure at constant gas velocity reaching up to 1.18 for the highest gas velocities.

These trends still lead to a variation of U_{mf} as a function of pressure similar to that observed for the powder alone (cf. Figure 8.a). Compared to the minimum fluidization velocities of the powder alone, the U_{mf} curve of the short fiber/powder mixture shifts globally towards higher minimum fluidization velocities. The minimum fluidization velocity (U_{mf}) increases as the pressure decreases: from 800 to 200 mbar, U_{mf} varies only little (from 39 cm.min^{-1} to 53 cm.min^{-1}) and below 200 mbar, U_{mf} increases very rapidly reaching up to 171 cm.min^{-1} at 10 mbar. At the highest and lowest pressures (beyond 400 mbar and below 50 mbar, respectively), ΔP_∞^* drops, either progressively at high pressures, or rapidly at low pressures. At intermediate pressures (from 100 to 400 mbar), the fluidization quality factor remains at a maximum. The optimum pressure for an efficient fluidization is therefore identified around 200 mbar where ΔP_∞^* is close to 1.

From the Ergün equation (cf. Equation 5) and the correlation of Zarekar *et al.* (cf. Equation 1), by fitting the equations to the experimental data, comes the two fitted effective particle diameters of $\psi_s d_g = 35.5 \pm 2.2$ µm and $\psi_s d_g = 83.5 \pm 3.5$ µm, respectively, which are difficult to correlate with the short fibers and the powder characteristics. The corresponding fitted equations are plotted in Figure 8.a in function of the pressure. Here again, the correlations are able to follow the experimental results at pressures above 200 mbar, but on the other hand, below 200 mbar, the correlations are not consistent with the experimental results. These two correlations lead to a mean relative error of 27%, with a maximum relative error of 69% at 10 mbar and a mean relative error of 23%, with a maximum relative error of 55% at 10 mbar, respectively.

The permeability (K) and Knudsen coefficient (D_k) were determined from the linear correlation of $\frac{Q}{S\Delta P}$ as a function of P_{mean} (cf. Equation 11), giving respectively $K = 8.60.10^{-12} \pm 4.88.10^{-13}$ m^2 and $D_K = 1.67.10^{-3} \pm$

$2.16.10^{-4}$ m^2s^{-1}. Assuming in this case a viscous tortuosity of $\eta_v = 6$ and $\eta_K = \left(\frac{\eta_v}{2,3}\right)^{\frac{1}{1,05}} = 2.49$ [71], for a porosity $\varepsilon_{mf} = 0.6$, the Kozeny-Carman equation (cf. Equations 18 and 19) leads to: $d_g = 32.5 \pm 1.8$ µm, from K and $d_g = 26.8 \pm 3.5$ µm, from D_k. The correlation is in good agreement with the experimental data and allows to predict U_{mf} with a mean relative error of 9% with a maximum relative error of 16% at 800 mbar.

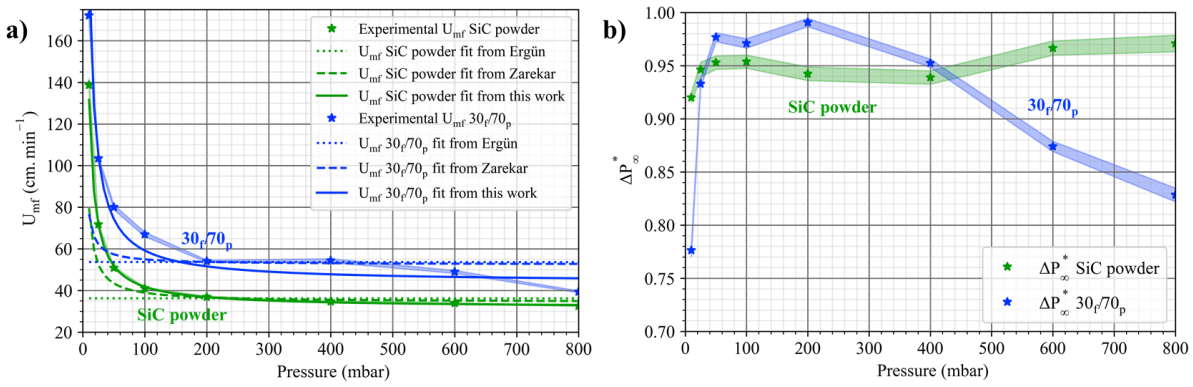

Figure 8 : a) Experimental minimum fluidization velocity (solid line) and calculated data (dotted lines) and b) quality factor as a function of pressure for the pure SiC powder and the $30_f/70_p$ mixture.

4.2. Effect of temperature

4.2.1. Powder

The determination of the pressure drop in the fixed bed area is particularly difficult and requires, to be correct, to keep the thermal homogeneity in the whole bed. To ensure this, the pressure drops near and below U_{mf} were determined by agitating the load at a speed much higher than U_{mf} for a few minutes and then by rapidly decreasing the gas flow to reach these low velocities. If the observed pressure drop is stable, the measurement is considered as correct.

The normalized pressure drops generated by the powder bed (cf. Figure 7.a) are affected by the variation of the temperature, especially on the pressure drop plateau at elevated gas velocities. The normalized bed pressure drop plateau (ΔP^*_∞) decreases with the rise of the temperature from 0.94 to 0.75 suggesting that the fluidization is not ideal at high temperature but maintained relatively stable to be compatible with a coating deposition process. On the contrary, the slopes of the initial linear parts remain constant. This results in a very small variation of the minimum fluidization velocity as a function of the temperature (cf. Figure 9.a). Such behavior is characteristic of small size particles as mentioned in the literature review (<100 µm). It is therefore possible, a priori, to use the minimum fluidization velocities obtained at room temperature also at high temperatures.

The equation of Ergün (cf. Equation 5) and the correlation proposed by Zarekar (cf. Equation 1) can be used again, this time involving temperature at fixed pressure. The calculations lead to an effective particle diameter of $\psi_s d_g = 77.0 \pm 5.7$ µm and $\psi_s d_g = 76.6 \pm 5.0$ µm respectively, which is relatively close to the actual powder particle diameter of $d_g = 71$ µm. The related equations are plotted in Figure 9.a. The equations do not correlate with the experimental data and deviate from what is expected at room temperature for high temperatures. With a mean relative error of 29% the correlation reaches a maximum relative error of 41% at 400°C using the Ergün equation

and a mean relative error of 26% the correlation reaches a maximum relative error of 43% at the highest temperature (1000°C) with the correlation of Zarekar *et al.* it is clear that the coefficients determined by Zarekar *et al.* can't be reused at temperatures above ambient.

Depending on the (P, T) conditions, K is supposed to be constant, whereas D_k is expected to vary proportionally to the square root of the temperature (cf. Equation 8). From the Darcy-Klinkenberg assumption, and with an adjustment of the variables, the values of the viscous (η_v) and Knudsen (η_K) tortuosities can be determined (cf. Equations 22 and 8). If the particle diameter $d_g = 71$ µm is fixed, then comes: $\eta_v = 9.92 \pm 0.49$ and $\eta_K = 1.67 \pm 0.07$. These values are consistent with those already found above. Moreover, these tortuosity values result in: $K = 3.07.10^{-12} \pm 1.53.10^{-13}$ m² and $D_K = 1.89.10^{-3} \pm 7.92.10^{-5}$ m²s^{-1} (at T = 25°C). The correlation is again in good agreement with the experimental data and allows a prediction of U_{mf} with a mean relative error of 2% and a maximum relative error of 5% at 200°C.

4.2.2. Powder and short fibers mixture

The normalized pressure drops (cf. Figure 7.b) are here again affected by the variation of the temperature. The first linear part of the curves (fixed bed area) remain unchanged as a function of the temperature. As for the powder, the pressure drop plateau at high gas velocities is affected by the temperature. The normalized bed pressure drop plateau (ΔP^*_∞) decreases with the rise of the temperature from 0.82 at room temperature to 0.69 at 1000°C. These values still allow us to consider coating deposition. As a result, a small variation of the minimum fluidization velocity with the temperature is observed (cf. Figure 9.a).

Fitted effective particle diameters of $\psi_s d_g = 36.8 \pm 1.5$ µm and $\psi_s d_g = 86.0 \pm 3.2$ µm were founded by varying the temperature at fixed pressure, with both Ergün equation (cf. Equation 5) and Zarekar *et al.* correlation (cf. Equation 1), respectively. These results are close to the particle effective diameters found before. The related fitted equations are plotted in Figure 9.a. The equations do not correlate with the experimental data. Ergün equation exhibits the maximum mean relative error with 47% against 17% for Zarekar *et al.* correlation. Both equations reach a maximum relative error of 74% and 24% at 1000°C, respectively. The coefficients determined by Zarekar *et al.* can't be reused at temperatures above ambient.

The particle diameter (d_g) can be determined from the Darcy-Klinkenberg assumption, with an adjustment of the variables (cf. Equations 22 and 8). If the viscous and Knudsen tortuosities are fixed: $\eta_v = 6$ and $\eta_K = 2.49$ [71], then comes: $d_g = 31.5 \pm 0.5$ µm. This value is consistent with that found previously. The correlation is again in good agreement with the experimental data and allows predicting U_{mf} with a mean relative error of only 6% and a maximum relative error of 14% at 1000°C.

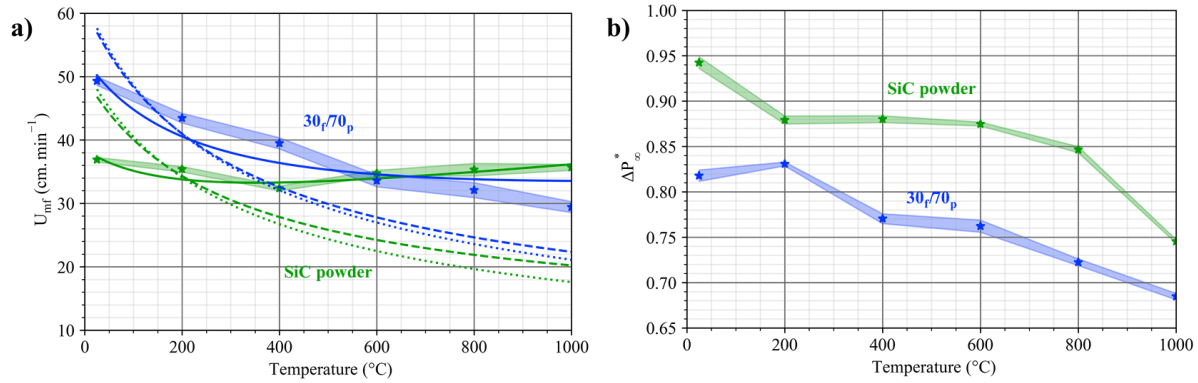

Figure 9 : a) Experimental minimum fluidization velocity (solid line) and calculated data (dotted lines) and b) quality factor as a function of temperature for the pure SiC powder and the $30_f/70_p$ mixture. Same legend as Figure 8.

4.1. Bed expansion

A prediction of the bed expansion of the same type as those proposed by Chitester *et al.* [35] and Lewis *et al.* [59] was applied, where $^{H}/_{H_{mf}}$ is a function of $1 + \alpha(U - U_{mf})\rho_g{}^{n_4}$. The α coefficient then contains the information specific to U_{mf}, ρ_p and d_g, while n_4 involves the variation of the expansion with pressure. Table 3 summarizes the results obtained.

Table 3 : Bed expansion correlations for the pure SiC powder and the $30_f/70_p$ mixture.

	SiC powder	$30_f/70_p$
α	3.56 ± 0.23	4.03 ± 0.32
n_4	0.1913 ± 0.0368	0.2303 ± 0.0257
Mean correlation coefficient	0.95283	0.94029

The correlated values of α and n_1 are difficult to exploit since they are very sensitive to the way the bed expansion equation is presented. However, the average correlation coefficient for the powder and the $30_f/70_p$ mixture are acceptable. For the $30_f/70_p$ mixture α and n_1 increase by 13% and 20% respectively compared to the values obtained for the powder alone. This indicates a greater expansion of the short fiber/powder mixture bed than the powder alone. This result is expected since short fibers have a higher Hausner ratio than powders alone. The share of short fibers in the mixture increases the expansion capacity of the mixture due to their particular geometry.

The correlations proposed in the literature (cf. Table 1) and those obtained from this study are calculated and compared to the experimental data for each pressure explored, for the pure powder and the $30_f/70_p$ mixture. In the case of the $30_f/70_p$ mixture, the correlations were calculated using the average diameter obtained previously (i.e. $d_g = 32.0$ µm). At each pressure, the normalized squared error (namely E_{L^2}) is determined according to the formula: $\sum_i (x_{corr,i} - x_{ex,i})^2 / \sum_i x_{ex,i}{}^2$, where $x_{corr,i}$ are the data deduced from the different correlations and $x_{ex,i}$ the experimental data. The results are gathered in Figure 10.

The correlation proposed by Lewis *et al.* [59] appears to be in closest agreement with the experimental data: it correctly predicts the expansion behavior of the powder and the $30_f/70_p$ mixture beds as a function of pressure.

The other correlations deviate from the expansions determined experimentally, especially those proposed by Feng *et al.* [58] and Rashid *et al.* [60].

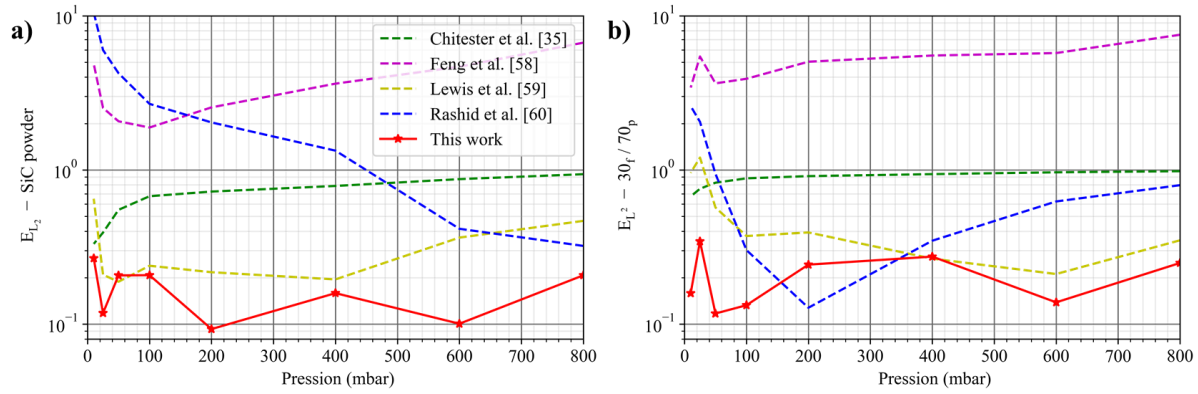

Figure 10 : Weighted squared errors as a function of pressure for a) the pure SiC powder and b) the 30$_f$/70$_p$ mixture.

4.2. Summary on pressure and temperature effects

This work intends to explore the effect of reduced pressure and temperature on the hydrodynamic behavior of a mixture of powder and short fibers. Under these working conditions and for the gas velocities necessary for the fluidization of such loads, the rarefied flows are not negligible while the inertial flows are. We chose to use our own equation (cf. Equation 22) considering the characteristics of the porous medium of the bed: particle diameter (d_g) and tortuosities (η_v and η_K), while the vast majority of studies prefer to use geometric considerations of individual particles: particle diameter (d_g) and sphericity (ψ_s). The Ergün equation (cf. Equation 5) and the correlation proposed by Zarekar *et al.* (cf. Equation 1) are compared to our equation. The results are gathered in Table 4.

The study looks first at the effect of the variation of the pressure at room temperature and then at the role of the temperature at P = 200 mbar. The Ergün equation and the correlation of Zarekar *et al.* approach the powder diameter in both cases. In the case of the mixture, the Zarekar *et al.* curve fitting indicates an equivalent particle diameter around 86 µm. It is then difficult to explicitly relate this value to the geometrical parameters of the powder and the short fibers. However, one can simply state that the addition of 30% tapped volume of short fibers in a powder load increases the equivalent diameter considered for the fluidization by about 15 µm. In summary, the Ergün equation and the correlation of Zarekar *et al.* are suitable for the prediction of U_{mf} at room temperature and relatively moderate pressures (above 200 mbar), but not at high temperatures or low pressures, where the equations deviate from the experimentally observed behavior. In the latter conditions, it would be necessary to redefine the coefficients of the Zarekar *et al.* correlation.

Table 4 : Results of equation fitting for pure SiC powder and $30_f/70_p$ mixture.

Equation / Correlation	Fitted parameters	Pressure (Isotherm: 25°C)		Temperature (Isobar: 200 mbar)	
		SiC powder	$30_f/70_p$	SiC powder	$30_f/70_p$
Ergün *(cf. Equation 5)*	$\psi_s d_g$ (µm)	66.9 ± 2.8	35.5 ± 2.2	77.0 ± 5.7	36.8 ± 1.5
	Mean relative error	24%	27%	29%	47%
	Max relative error	74% (at 10 mbar)	69% (at 10 mbar)	41% (at 400°C)	74% (at 1000°C)
Zarekar *et al.* *(cf. Equation 1)*	$\psi_s d_g$ (µm)	67.6 ± 1.2	83.5 ± 3.5	76.6 ± 5.0	86.0 ± 3.2
	Mean relative error	13%	23%	26%	17%
	Max relative error	43% (at 10 mbar)	55% (at 10 mbar)	43% (at 1000°C)	24% (at 1000°C)
This work *(cf. Equation 23)*	K ($10^{-12}m^2$)	4.05 ± 0.03	8.60 ± 0.49	3.07 ± 0.15	9.26 ± 0.21
	D_K ($10^{-3}m^2.s^{-1}$)	0.71 ± 0.02	1.67 ± 0.22	1.89 ± 0.08 (calculated at 25°C)	0.29 ± 0.01 (calculated at 25°C)
	ε_{mf}	0.4**	0.6**	0.4*	0.6*
	d_g (µm)	71.0*	32.5 ± 1.8 from K 26.8 ± 3.5 from D_K	71.0*	31.5 ± 0.5
	η_v	7.52 ± 0.06	6.00*	9.92 ± 0.49	6.00*
	η_K	4.42 ± 0.13	2.49*	1.67 ± 0.07	2.49*
	Mean relative error	2%	9%	2%	6%
	Max relative error	5% (at 10 mbar)	16% (at 800 mbar)	5% (at 200°C)	14% (at 1000°C)

* = Fixed parameter (supposed)

** = Fixed parameter (experimentally calculated)

Considering this time Equation 22 and the parameter fitting on the experimental data it was possible to determine accurately the variation of U_{mf} at reduced pressure and high temperature. Equation 22 allowed to determine the characteristics of the porous medium assuming the particle diameter, in the case of the powder and reciprocally, the equivalent particle diameter assuming the characteristics of the porous medium, in the case of the short fiber/powder mixture. The powder tortuosities results show an increase in the viscous tortuosity and a decrease in the Knudsen tortuosity between the isothermal and isobaric results. For the short fiber/powder mixture assuming the tortuosity values, the equivalent particle diameter remains consistent and equal to 33 µm on average. These results are consistent with those obtained by fitting the Ergün equation. However, it is again difficult to link these equivalent particle diameters to the geometric characteristics of the powder and short fibers. The addition of 30% tapped volume of short fibers reduces the equivalent particle diameter by about 38 µm compared to the powder diameter. Compared to the correlation of Zarekar *et al.*, our equation allows a fine prediction of U_{mf} on the whole range of pressure and temperature explored.

4.3. CVD coating on short fiber/powder mixture

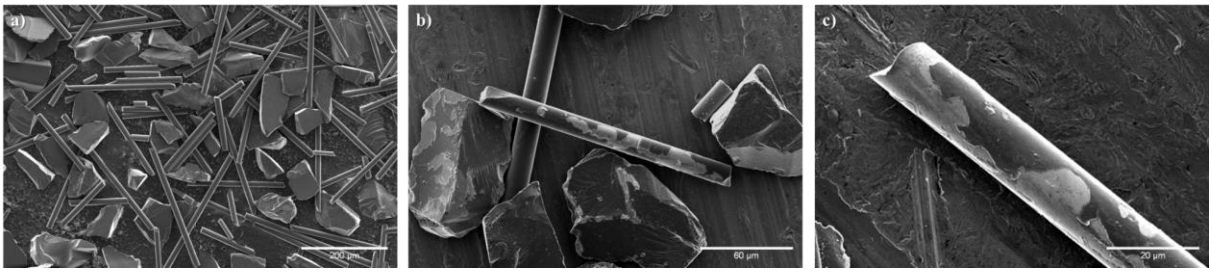

Figure 11 : SEM micrographs of pyC coated $30_f/70_p$ mixture a) general view of the intact mixture, b) and c) intentionally flaked mixture.

In order to evaluate the hydrodynamic study of the mixture of short fibers and powder in reactive conditions, a CVD experiment was carried out under conditions close to the previous study. The pressure was set at 200 mbar, for an optimal fluidization and the temperature at 1000°C. As above, the increase of the temperature resulted in a decrease of the fluidization quality, but it was sufficient to perform CVD in stable conditions for 12 hours. The gas velocity was set at five times U_{mf} to limit the influence of the precursor on the fluidization process. The deposition was achieved on a 400 g load of a $30_f/70_p$ mixture, with nitrogen as carrier gas and ethanol as carbon precursor. The molar ratio between the nitrogen and ethanol was set at 9 for a total gas flow rate of 248 $cm.min^{-1}$. Although the nature of the gas is different, the consequences of the ethanol addition on the temperature and the fluidization behavior of the bed is limited. The precursor is indeed highly diluted in nitrogen, the enthalpies of the pyrolysis and deposition reactions are relatively low (e.g. compared to combustion reactions) and the kinetics and yield of the pyrocarbon deposition are also very low (less than 16 $nm.h^{-1}$). The temperature recorded at the center of the bed during deposition indeed revealed changes of less than 1 or 2 % from pure N_2 to the reactive mixture.

The coated particles are shown in Figure 11. Multiple scanning electron microscopy analysis confirms that the coating is uniform, adherent and covers the entire surface of the short fibers and powders (cf. Figure 11.a). The mixture was voluntarily partially crushed to reveal the flaked coating, which appears dark on the surface of the short fiber and powder substrate (cf. Figure 11.b and c.). Scanning electron microscopy and thermogravimetric analyses revealed a pyrolytic carbon coating thickness of 190 nm representing 1.88% ± 0.01 by mass.

These experimental analyses have shown that the fluidization quality slightly degrades with increasing temperature, under both nitrogen and reactive gas. However, they have allowed the selection of an optimal operating point, which ensures a stable fluidization regime suitable for a CVD coating. The detrimental effect of the temperature, not yet explained, could be due to other aspects than purely hydrodynamic factors. For objects as small, lightweight and elongated as fibers, physico-chemical parameters such as inter-fiber cohesion could also play an important role, especially in the case of a high fiber proportion mixtures. However, it should be noted that a very good coating uniformity can be obtained even under non-ideal fluidization conditions, which demonstrates the robustness of the FB-CVD process on short fibers.

5. Conclusion

Our study has demonstrated the possibility of fluidizing a mixture of short Hi Nicalon S fibers and SiC powder. The parametric pressure/temperature study revealed a hydrodynamic behavior that required a rewriting of the Ergün law considering the description of laminar/rarefied flows. This hydrodynamic law is based on the diameters of the fluidized particles and the tortuosity generated by such load. Particularly adapted at low pressures (bellow 100 mbar), the Darcy's law corrected by the Klinkenberg effect was found to correlate well with the experimental

data. It was also possible to propose equivalent tortuosity values for the powder as well as equivalent particle size for the short fiber/powder mixture.

The experimental study of the minimum fluidization velocity U_{mf} and the fluidization quality factor as a function of pressure revealed that the fluidization behavior is optimal within the range 100-400 mbar. Below 100 mbar, the slip-flow effect predominates and tends to decrease the fluidization quality factor and drastically increase U_{mf}, whereas under 400 mbar the quality factor of short fiber/powder mixture decreases.

The study as a function of temperature revealed very small variations in U_{mf} allowing the use of the observations made at room temperature also at high temperatures, with very small error. On the other hand, the study also showed a quality factor of fluidization which decreases at high temperature probably indicating a phenomenon of partial channeling or an increase of the interparticle forces.

The proposed correlations for the expansions of the powder beds and the short fiber/powder mixture provide a link between the expansion, the difference between the velocity and the minimum fluidization velocity ($U - U_{mf}$) and the gas density (ρ_g). Although the previous correlations do not allow to describe a general dependence between the bed expansion and the gas density for example, that proposed by Lewis *et al.* [59] seems to give the best approximation of the behavior of a powder or short fiber/powder mixture bed for all pressures explored in this work.

This work ultimately demonstrated that the fluidization of original loads such as short fibers could be applied for CVD conditions. An ex-ethanol pyrolytic carbon coating was successfully deposited, of uniform thickness and covering the entire surface of individual short fibers and powders.

Acknowledgements

The authors are indebted to Sébastien Couthures and Rémi Bouvier for their contribution in the development and maintenance of the fluidized bed reactor. The authors thank Christine Rey-Rouch from LGC-SAP in Toulouse and Helga Mayr from IDM Systems in Darmstadt for the particle size analysis. The grant awarded by the University of Bordeaux and the operating support provided by Safran Ceramics are both gratefully acknowledged.

Declaration of interests

The authors declare that they have no known competing financial interests or personal relationships that could have appeared to influence the work reported in this paper.

References

[1] Brewer D. HSR/EPM combustor materials development program. Mater Sci Eng A 1999;261:284–91. https://doi.org/10.1016/S0921-5093(98)01079-X.

[2] Marshall DB, Evans AG. Failure Mechanisms in Ceramic-Fiber/Ceramic-Matrix Composites. J Am Ceram Soc 1985;68:225–31. https://doi.org/10.1111/j.1151-2916.1985.tb15313.x.

[3] DiCarlo JA, van Roode M. Ceramic Composite Development for Gas Turbine Engine Hot Section Components. GT2006, Volume 2: Aircraft Engine; Ceramics; Coal, Biomass and Alternative Fuels; Controls, Diagnostics and Instrumentation; Environmental and Regulatory Affairs: 2006, p. 221–31. https://doi.org/10.1115/GT2006-90151.

[4] Caussat B, Hemati M, Couderc JP. Silicon deposition from silane or disilane in a fluidized bed—Part I: Experimental study. Chem Eng Sci 1995;50:3615–24. https://doi.org/10.1016/0009-2509(95)00172-2.

[5] Tap R, Willert-Porada M. Dual PE-CVD Circulating Fluidized Bed Reactor. IEEE Trans Plasma Sci 2004;32:2085–92. https://doi.org/10.1109/TPS.2004.835969.

[6] Gerdes T, Tap R, Bahke P, Willert-Porada M. CVD-Processes in Microwave Heated Fluidized Bed Reactors. Adv. Microw. Radio Freq. Process., Berlin, Heidelberg: Springer Berlin Heidelberg; 2006, p. 720–34.

[7] Williams BE, Stiglich J. Hafnium- and Titanium-Coated Tungsten Powders for Kinetic Energy Penetrators, Phase 1, SBIR. Ultramet Pacoima Ca; 1992.

[8] Lin H-T, Huang J-L, Lo W-T, Wei W-CJ. Investigation on Carbonizing Behaviors of Nanometer-sized Cr2O3 Particles Dispersed on Alumina Particles by Metalorganic Chemical Vapor Deposition in Fluidized Bed. J Mater Res 2005;20:2154–60. https://doi.org/10.1557/JMR.2005.0268.

[9] Cadoret L, Reuge N, Pannala S, Syamlal M, Rossignol C, Dexpert-Ghys J, et al. Silicon Chemical Vapor Deposition on macro and submicron powders in a fluidized bed. Powder Technol 2009;190:185–91. https://doi.org/10.1016/j.powtec.2008.04.083.

[10] Rodriguez P, Caussat B, Ablitzer C, Iltis X, Brothier M. Fluidization and coating of very dense powders by Fluidized Bed Chemical Vapour Deposition. Chem Eng Res Des 2013;91:2477–83. https://doi.org/10.1016/j.cherd.2012.11.007.

[11] Kouadri-Mostefa S, Serp P, Hémati M, Caussat B. Silicon Chemical Vapor Deposition (CVD) on microporous powders in a fluidized bed. Powder Technol 2001;120:82–7. https://doi.org/10.1016/S0032-5910(01)00351-5.

[12] El Mansouri A. Développement de la technologie CVD à lit fluidisé pour l'enrobage de poudres céramiques par du pyrocarbone. PhD Thesis. Bordeaux, 2021.

[13] Yates JG, Lettieri P. Fluidized-Bed Reactors: Processes and Operating Conditions. 1st ed. 2016. Cham: Springer International Publishing : Imprint: Springer; 2016.

[14] Pajkic Z, Willert-Porada M. Atmospheric pressure microwave plasma fluidized bed CVD of AlN coatings. Surf Coat Technol 2009;203:3168–72. https://doi.org/10.1016/j.surfcoat.2009.03.047.

[15] Pontiller P, Willert-Porada M. High Temperature Behavior of Si3N4 and Yb2SiO5 Coated Carbon Fibers for Silicon-Nitride CMC: High Temperature Behavior of Si3N4 and Yb2SiO5. Adv Eng Mater 2014;16:556–64. https://doi.org/10.1002/adem.201300443.

[16] Zhong W-Q, Zhang Y, Jin B-S, Zhang M-Y. Discrete Element Method Simulation of Cylinder-Shaped Particle Flow in a Gas-Solid Fluidized Bed. Chem Eng Technol 2009;32:386–91. https://doi.org/10.1002/ceat.200800516.

[17] Hilton JE, Mason LR, Cleary PW. Dynamics of gas–solid fluidised beds with non-spherical particle geometry. Chem Eng Sci 2010;65:1584–96. https://doi.org/10.1016/j.ces.2009.10.028.

[18] Zhou ZY, Pinson D, Zou RP, Yu AB. Discrete particle simulation of gas fluidization of ellipsoidal particles. Chem Eng Sci 2011;66:6128–45. https://doi.org/10.1016/j.ces.2011.08.041.

[19] Chen X, Zhong W, Heindel TJ. Fluidization of cylinder particles in a fluidized bed. Adv Powder Technol 2017;28:820–35. https://doi.org/10.1016/j.apt.2016.12.008.

[20] Boer L, Buist KA, Deen NG, Padding JT, Kuipers JAM. Experimental study on orientation and de-mixing phenomena of elongated particles in gas-fluidized beds. Powder Technol 2018;329:332–44. https://doi.org/10.1016/j.powtec.2018.01.083.

[21] Zhong L, Xu D, Jiang Y, Guo Y. A numerical study on gas-fluidized beds of wet flexible fibers. Powder

Technol 2022;399:117094. https://doi.org/10.1016/j.powtec.2021.117094.

[22] Leturia M, Saleh K. Fluidisation gaz-solide Particules fines et nanoparticules. Tech Ing 2016;base documentaire : TIP452WEB. https://doi.org/10.51257/a-v1-j4101.

[23] Dutta A, Dullea LV. Effects of external vibration and the addition of fibers on the fluidization of a fine powder. AIChE Symp Ser, vol. 87, 1991, p. 38–46.

[24] Alavi S, Caussat B. Experimental study on fluidization of micronic powders. Powder Technol 2005:7.

[25] Zhou T, Li H. Effects of adding different size particles on fluidization of cohesive particles. Powder Technol 1999;102:215–20. https://doi.org/10.1016/S0032-5910(98)00211-3.

[26] Liu Y-D, Kimura S. Fluidization and entrainment of difficult-to-fluidize fine powdermixed with easy-to-fluidize large particles. Powder Technol 1993;75:189–96.

[27] Sidorenko I, Rhodes MJ. Influence of pressure on fluidization properties. Powder Technol 2004;141:137–54. https://doi.org/10.1016/j.powtec.2004.02.019.

[28] Sidorenko I, Rhodes MJ. Pressure Effects on Gas-Solid Fluidized Bed Behavior. Int J Chem React Eng 2003;1. https://doi.org/10.2202/1542-6580.1107.

[29] Yates JG. Effects of temperature and pressure on gas-solid fluidization. Chem Eng Sci 1996;51:167–205. https://doi.org/10.1016/0009-2509(95)00212-X.

[30] Rowe PN, Foscolo PU, Hoffmann AC, Yates JG. X-ray observation of gas fluidized beds under pressure. Fluid IV 1984:p 53.

[31] Ergun S, Orning AA. Fluid Flow through Randomly Packed Columns and Fluidized Beds. Ind Eng Chem 1949;41:1179–84. https://doi.org/10.1021/ie50474a011.

[32] Wen CY, Yu YH. A generalized method for predicting the minimum fluidization velocity. AIChE J 1966;12:610–2. https://doi.org/10.1002/aic.690120343.

[33] Bourgeois P, Grenier P. The ratio of terminal velocity to minimum fluidising velocity for spherical particles. Can J Chem Eng 1968;46:325–8. https://doi.org/10.1002/cjce.5450460508.

[34] Babu S. P, Shah B, Talwalkar A. Fluidization correlations for coal gasification materials - Minimum fluidization velocity and fluidized bed expansion ratio. AIChE Symp Ser Am Inst Chem Eng 1978;74:176–86.

[35] Chitester DC, Kornosky RM, Fan L-S, Danko JP. Characteristics of fluidization at high pressure. Chem Eng Sci 1984;39:253–61. https://doi.org/10.1016/0009-2509(84)80025-1.

[36] Tannous K, Hemati M, Laguerie C. Caractéristiques au minimum de fluidisation et expansion des couches fluidisées de particules de la catégorie D de Geldart. Powder Technol 1994;80:55–72.

[37] Fletcher JV, Deo MD, Hanson FV. Fluidization of a multi-sized group B sand at reduced pressure. Powder Technol 1993;76:141–7. https://doi.org/10.1016/S0032-5910(05)80021-X.

[38] Kusakabe K, Kuriyama T, Morooka S. Fluidization of Fine Particles at Reduced Pressure 1989:125–30.

[39] Huschka H, Popp W. Coating of feed-and breed-particles in a fluidised bed under reduced pressure. J Nucl Mater 1967;23:109–10.

[40] Germain B, Claudel B. Fluidization at mean pressures less than 30 Torr. Powder Technol 1975;13:115–21.

[41] Kawamura Y. The Flow of Gas in a Fluidized Bed at Low Pressure. Kagaku Kogaku 1961;25:524–9.

[42] Zarekar S, Bück A, Jacob M, Tsotsas E. Reconsideration of the hydrodynamic behavior of fluidized beds operated under reduced pressure. Powder Technol 2016;287:169–76.

https://doi.org/10.1016/j.powtec.2015.09.027.

[43] Llop MF, Madrid F, Arnaldos J, Casal J. Fluidization at vacuum conditions. A generalized equation for the prediction of minimum fluidization velocity. Chem Eng Sci 1996;51:5149–57. https://doi.org/10.1016/S0009-2509(96)00351-X.

[44] Kunii D, Levenspiel O, Brenner H. Fluidization Engineering. Elsevier Science; 1991.

[45] Yates JG. Effects of temperature and pressure on gas-solid fluidization n.d.:41.

[46] Subramani HJ, Mothivel Balaiyya MB, Miranda LR. Minimum fluidization velocity at elevated temperatures for Geldart's group-B powders. Exp Therm Fluid Sci 2007;32:166–73. https://doi.org/10.1016/j.expthermflusci.2007.03.003.

[47] Shao Y, Gu J, Zhong W, Yu A. Determination of minimum fluidization velocity in fluidized bed at elevated pressures and temperatures using CFD simulations. Powder Technol 2019;350:81–90. https://doi.org/10.1016/j.powtec.2019.03.039.

[48] Chirone R, Poletto M, Barletta D, Lettieri P. The effect of temperature on the minimum fluidization conditions of industrial cohesive particles. Powder Technol 2020;362:307–22. https://doi.org/10.1016/j.powtec.2019.11.102.

[49] Botterill JSM, Teoman Y, Yüregir KR. Comments on "comparison of commonly used correlations for minimum fluidization velocity of small solid particles." Powder Technol 1981;30:95–6. https://doi.org/10.1016/0032-5910(81)85031-0.

[50] Saxena SC, Grewal NS. Reply to comments on 'comparison of commonly used correlations for minimum fluidization velocity of small solid particles.' Powder Technol 1981;30:96. https://doi.org/10.1016/0032-5910(81)85032-2.

[51] Raso G, D'Amore M, Formisani B, Lignola PG. The influence of temperature on the properties of the particulate phase at incipient fluidization. Powder Technol 1992;72:71–6. https://doi.org/10.1016/S0032-5910(92)85023-O.

[52] Peters MH, Fan L-S, Sweeney TL. Reactant dynamics in catalytic fluidized bed reactors with flow reversal of gas in the emulsion phaset. Chem Eng Sci 1982;37:553–65. https://doi.org/10.1016/0009-2509(82)80118-8.

[53] Shen CY, Johnstone HF. Gas-solid contact in fluidized beds. AIChE J 1955;1:349–54. https://doi.org/10.1002/aic.690010313.

[54] Hilligardt K, Werther J. Local bubble gas hold-up and expansion of gas/solid fluidized beds. Chem Ing Tech 1985;57:622–3. https://doi.org/10.1002/cite.330570713.

[55] Xavier AM, Lewis DA, Davidson JF. Expansion of bubbling fluidised beds. Trans Inst Chem Eng 1978;56:274–80.

[56] Agu CE, Tokheim L-A, Eikeland M, Moldestad BME. Improved models for predicting bubble velocity, bubble frequency and bed expansion in a bubbling fluidized bed. Chem Eng Res Des 2019;141:361–71. https://doi.org/10.1016/j.cherd.2018.11.002.

[57] Geldart D. Expansion of Gas Fluidized Beds. Ind Eng Chem Res 2004;43:5802–9. https://doi.org/10.1021/ie040180b.

[58] Feng R, Li J, Cheng Z, Yang X, Fang Y. Influence of particle size distribution on minimum fluidization velocity and bed expansion at elevated pressure. Powder Technol 2017;320:27–36. https://doi.org/10.1016/j.powtec.2017.07.024.

[59] Lewis WK, Gilliland ER, Bauer WC. Characteristics of Fluidized Particles. Ind Eng Chem 1949;41:1104–17. https://doi.org/10.1021/ie50474a004.

[60] Rashid TAB, Zhu L-T, Luo Z-H. Comparative analysis of numerically derived drag models for development of bed expansion ratio correlation in a bubbling fluidized bed. Adv Powder Technol 2020;31:2723–32. https://doi.org/10.1016/j.apt.2020.04.036.

[61] Klinkenberg LJ. The Permeability Of Porous Media To Liquids And Gases, 1941.

[62] Carman PC. Fluid flow through granular beds. Chem Eng Res Des 1997;75:S32–48. https://doi.org/10.1016/S0263-8762(97)80003-2.

[63] Epstein N. On tortuosity and the tortuosity factor in flow and diffusion through porous media. Chem Eng Sci 1989;44:777–9. https://doi.org/10.1016/0009-2509(89)85053-5.

[64] Wadell H. Volume, Shape, and Roundness of Rock Particles. J Geol 1932;40:443–51. https://doi.org/10.1086/623964.

[65] El Mansouri A, Bertrand N, Couthures S, Guette A. Apparatus for Fluidized-Bed Chemical Vapour Deposition. WO2022003268 (A1), 2022.

[66] Davidson JF, Harrison D. Fluidised Particles. Cambridge University Press; 1st edition; 1963.

[67] Leturia M, Saleh K. Fluidisation gaz-solide Bases et théorie. Tech Ing 2014;base documentaire : TIP452WEB. https://doi.org/10.51257/a-v2-j4100.

[68] Beddow JK. Professor Dr. Henry H. Hausner, 1900–1995. Part Part Syst Charact 1995;12:213–213. https://doi.org/10.1002/ppsc.19950120411.

[69] Jacquelin M. Etude de la mise en suspension de particules par chute de poudre. PhD Thesis. Université Paris XII - Val de Marne, 2007.

[70] Tea J. Evaluation de la coulabilité des poudres comparaison de méthodes de mesure. PhD Thesis. Université de Lorraine, 2015.

[71] Charles C, Descamps C, Vignoles GL. Low pressure gas transfer in fibrous media with progressive infiltration: correlation between different transfer modes. Int J Heat Mass Transf 2022;182:121954. https://doi.org/10.1016/j.ijheatmasstransfer.2021.121954.

Vitae

Thomas Da Calva is a Ph.D. student in the development of ceramic coatings on short fibers by Fluidized Bed CVD process in the ThermoStructural Composites Laboratory since 2020. Graduated from the National Engineering School of Tarbes, France in the speciality of Structural Materials and Processes Engineering, Thomas Da Calva also holds a double degree in Materials Processing Characterization and Surface Treatments in partnership with the National School of Chemical and Technological Arts Engineers and the Paul Sabatier University of Toulouse.

Clément Rivière is a student at the University of Bordeaux in the Master of Advanced Materials. The training is centered around polymeric, metallic and ceramic materials from their elaboration/design, their physico-chemical characterizations to their use in specific functions/applications. As an intern in the LCTS for 2 months, he worked on pyrolytic carbon coatings by FB-CVD. Wishing to work in the field of materials engineering, Clément would like to pursue a career in motorsports material engineering.

Georges Chollon is research scientist at the French National Center for Scientific Research (CNRS) since 1999. He graduated from the National School of Physics and Chemistry of Bordeaux in 1990 and obtained a Ph.D. in Materials Science from the University of Bordeaux in 1995. He completed two post-doctoral fellowships, at EMPA-Dübendorf, Switzerland, in 1995-1996 and NIMCR-Tsukuba, Japan, in 1996-1998. At LCTS, he is investigating the relationships between synthesis (mainly by CVD), composition, structure and properties of carbon and non-oxide ceramics.

Gérard L. Vignoles is a professor of the University of Bordeaux, hired since 1994 and is head of the ThermoStructural Composites Laboratory since 2016 and of the French CNRS research group (GDR) "(CMC)²" since 2019. His main topics of interest encompass physico-chemical modeling of thermostructural composite fabrication processes, mechanical, thermal and ablative behavior.

Nathalie Bertrand is an Assistant Professor in the Chemistry Department of the University of Bordeaux since 2003. She completed a Ph.D. in Chemical engineering in 2001 at Toulouse INP. Her main topics of interest concern Gaseous fluidization, Transport phenomena and Chemical Vapor Deposition. Her current research activities focus on the use of Fluidized Bed-CVD process on short fibers.